Amplified melt and flow of the Greenland ice sheet driven by late-summer cyclonic rainfall

Doyle, Sam; Hubbard, Alun; van de Wal, Roderik; Box, Jason ; van As, Dirk; Scharrer, Killian; Meierbachtol, Toby; Smeets, Paul ; Harper, Joel; Johansson, Emma ; Mottram, Ruth; Mikkelsen, Andreas; Wilhelms, Frank; Patton, Henry; Christoffersen, Poul; Hubbard, Bryn

Published in:
Nature Geoscience

DOI:
10.1038/NGEO2482

Publication date:
2015

Citation for published version (APA):
Doyle, S., Hubbard, A., van de Wal, R., Box, J., van As, D., Scharrer, K., Meierbachtol, T., Smeets, P., Harper, J., Johansson, E., Mottram, R., Mikkelsen, A., Wilhelms, F., Patton, H., Christoffersen, P., & Hubbard, B. (2015). Amplified melt and flow of the Greenland ice sheet driven by late-summer cyclonic rainfall. *Nature Geoscience*, *8*(8), 647-653. https://doi.org/10.1038/NGEO2482

This is the author's post-print. The final version was first published by Nature Geoscience on 13 July 2015, doi: 10.1038/NGEO2482

Amplified melt and flow of the Greenland ice sheet driven by late-summer cyclonic rainfall

Samuel H. Doyle[1*], Alun L. Hubbard[2,1], Roderik S.W. van de Wal[3], Jason E. Box[4,5], Dirk van As[4], Kilian Scharrer[6], Toby W. Meierbachtol[7], Paul C.J.P. Smeets[3], Joel T. Harper[7], Emma Johansson[8,9], Ruth H. Mottram[10], Andreas B. Mikkelsen[11], Frank Wilhelms[12,13], Henry Patton[2], Poul Christoffersen[14], and Bryn Hubbard[1]

[1]Centre for Glaciology, Department of Geography & Earth Sciences, Aberystwyth University, Aberystwyth, SY23 3DB, UK.
[2] Centre for Arctic Gas Hydrate, Environment and Climate, Department of Geology, The Arctic University of Norway, Tromsø, Norway
[3]Institute for Marine and Atmospheric research Utrecht, Utrecht University, P.O. Box 80005, 3508TA Utrecht, Netherlands.
[4]Geological Survey of Denmark and Greenland, Øster Voldgade 10, 1350 Copenhagen K, Denmark.
[5]Department of Geography, The Ohio State University, 1036 Derby Hall, 154 North Oval Mall, Columbus, Ohio, 43210-1361, USA.
[6]ENVEO IT GmbH, Innsbruck, Austria.
[7]Department of Geosciences, University of Montana, Missoula, Montana 59812, USA.
[8]Department of Physical Geography and Quaternary Geology, Bert Bolin Centre for Climate Research, Stockholm University, SE-106 91, Stockholm, Sweden.
[9]Swedish Nuclear Fuel and Waste Management Co, Box 250, 101 24, Stockholm.
[10]Danish Meteorological Institute, Lyngbyvej 100, DK-2100 Copenhagen Ø Denmark
[11]Department of Geosciences and Natural Resource Management, University of Copenhagen, Øster Voldgade 10, DK-1350 Copenhagen, Denmark.
[12]Alfred-Wegener-Institut Helmholtz-Zentrum für Polar- und Meeresforschung, Am Handelshafen 12, 27570 Bremerhaven Germany
[13]Department of Crystallography, Geoscience Centre, University of Göttingen, Goldschmidtstraße 1, 37077 Göttingen, Germany
[14]Scott Polar Research Institute, University of Cambridge, Lensfield Road, Cambridge, CB2 1ER, UK

*Please address e-mail correspondence to: sdd08@aber.ac.uk

9 June 2015

Intense rainfall events significantly affect Alpine and Alaskan glaciers through enhanced melting, ice flow acceleration and subglacial sediment erosion, yet their impact on the

This is the author's post-print. The final version was first published by Nature Geoscience on 13 July 2015, doi: 10.1038/NGEO2482

Greenland ice sheet has not been assessed. Here we present measurements of ice velocity, subglacial water pressure and meteorological variables from the western margin of the Greenland ice sheet during a week of warm, wet cyclonic weather in late-August and early-September 2011. We find that extreme surface runoff from melt and rainfall led to a widespread ice flow acceleration that extended 140 km into the ice sheet interior. We argue that the late-season timing was critical to promoting rapid runoff across an extensive bare ice surface, which overwhelmed a subglacial hydrological system in transition to a less-efficient winter mode. Reanalysis data reveal that the cyclonic weather conditions driving the event prevailed across southern and western Greenland, and a corresponding flow response was observed at all land- and marine-terminating glaciers in these regions with available data. Given that the advection of warm, moist air masses and rainfall over Greenland is expected to become more frequent in the coming decades, our findings portend a previously unforeseen vulnerability of the Greenland ice sheet to climate change.

The Greenland ice sheet (GrIS) is the largest cryospheric contributor to global sea-level rise: responsible for 0.7 mm yr^{-1} – a rate at least double that of the Antarctic ice sheets combined and one that has steadily accelerated over the last two decades[1,2]. Approximately half of this mass-loss is attributed to summer, surface melt processes enhanced through a number of positive feedbacks, such as surface albedo and hypsometry that are relatively well-constrained and amenable to modelling under future climate change[1,3]. The remaining dynamic mass losses are attributed to increased ice discharge and are clearly significant yet remain poorly constrained and difficult to model and predict[2]. Here we present evidence for a large, late-summer, cyclonically-induced runoff event that falls outside of the surface melt processes currently included in mass-

This is the author's post-print. The final version was first published by Nature Geoscience on 13 July 2015, doi: 10.1038/NGEO2482

loss assessments, and which had a potent and widespread effect on surface melt and ice dynamics.

In this study, we test the hypothesis that late-season cyclonic weather systems – which are predicted to increase in frequency and magnitude[4,5] yet have so far been neglected in studies of GrIS dynamics and mass balance[1,2] – produce sufficient runoff to overwhelm the ice sheet's basal drainage system, driving transient, widespread accelerations in ice flow. We focus our investigation on the Kangerlussuaq sector of the GrIS where a dense network of global positioning system (GPS) receivers and automated weather stations (AWS), plus borehole water-pressure and proglacial discharge records, enable a comprehensive analysis of the meteorological and glaciological conditions driving a late-season acceleration event in 2011. We then use reanalysis data to determine the synoptic weather and spatial footprint of this specific event, before interrogating meteorological, regional climate modelling and ice surface velocity records from around Greenland to determine the magnitude, impact, and frequency of this and other similar events in the past. This analysis provides a framework for the reinterpretation of three well-documented ice flow acceleration events that were previously incorrectly attributed to surface melt alone. Finally, we discuss the implications of these findings in the context of predicted changes in Greenland's climate over the next century.

Runoff and ice dynamics in the Kangerlussuaq Sector

Seasonal and inter-annual acceleration of GrIS flow is governed by the dynamic response of the basal hydrological system to variability in melt water delivery to the bed[6-14]. The highest ice velocities typically occur shortly after melt onset, when an inefficient drainage system is

This is the author's post-print. The final version was first published by Nature Geoscience on 13 July 2015, doi: 10.1038/NGEO2482

overwhelmed by the first major inputs of surface water of the melt season, with the lowest velocities usually observed in late summer and autumn when declining melt inputs are easily accommodated by an efficient and well-developed basal hydrological system[7-11].

The seasonal velocity cycle recorded at nine GPS sites on Russell Glacier and Isunngata Sermia in West Greenland during 2011 (Fig. 1) are consistent with these systematic variations with one exception: a prominent flow acceleration between the 24 August and 1 September (Fig. 2d,e). Surface velocities derived from offset tracking with TanDEM-X data show widespread acceleration of up to 220% across a large portion of the ice sheet margin for the interval 23 August to 3 September compared to the preceding period (1 to 23 August; Figs. 1 and S1). During the event, velocities at Russell Glacier GPS sites R2, R13, R38, R52 and R88 (where the number denotes kilometres from the glacier's terminus) increased by 117%, 140%, 71%, 64% and 46% above those of the preceding week (Table S1). The acceleration was particularly large at site R13 (Fig. 2d) where the daily mean velocity of 365 m yr^{-1} during the event exceeded the site's melt onset peak of 337 m yr^{-1} on 8 June, which typically represents the highest velocity within any given year[7,8,11]. The pronounced flow response was present across all neighbouring glaciers, including Isunngata Sermia, which accelerated by 22%, 58% and 55% at I14, I27 and I46 respectively (Figs. 1 and 2d; Table S1), and was also detectable – albeit muted – 140 km into the ice sheet interior, well within the accumulation zone at R140 (Fig. 2e).

We ascribe this flow acceleration to an intense period of surface runoff composed of both rainfall and melt. Measured rainfall during the event accounted for 20% (23.6 mm) of the annual total (115.1 mm) and despite such rainfall being uncommon for the Kangerlussuaq region[15], surface melt was the primary contributor to runoff. Furthermore, although the highest melt rates

during the event (e.g. 3.2 mm w.e. h^{-1} at M13 on 27 August, Fig. 3b) were less than peak summer values (e.g. 6 mm w.e. h^{-1} at M13 on 30 July 2011), they were unusually sustained throughout both day and night by enhanced longwave radiation and turbulent heat fluxes[16,17] associated with the advection of warm, moist air into the region (Figs. 3, 4, and S2; see extended online methods Section 4). This unusually sustained period of continuous melt totalled 331 mm water equivalent (w.e.) at M13 between 24 August and 1 September, representing 10% of the annual total and twice that of the preceding week (Fig. 3b). Given the upper estimate of rainfall of 24 mm, ice surface melt accounted for at least 93% of the overall runoff at M13 (732 m above sea level; asl) during the event. Measured melt was only slightly lower at higher-elevations: at M61 (1280 m asl) 315 mm w.e. of melt during the event accounted for a disproportionate percentage (15%) of the annual total (Fig. 2b). Melting extended throughout the entire ablation area beyond the mean (1990 - 2011) equilibrium line altitude (ELA)[18] of 1553 m asl. Although rain-induced ice melt was minimal at M13 (1.1 to 1.8 mm w.e.) the heat released by rain freezing into the surface snowpack enhanced melt above the snowline (1696 m asl). For instance, 14 mm of rain at 2° C freezing in the snowpack would bring 15 cm w.e. of snow at −15° C to the melting point (see extended online methods Section 4). At site M140 (1840 m asl), situated well above the snowline, 50 mm w.e. of melt (8% of the annual total) was recorded between 24 - 29 August, concurrent with above-freezing air temperatures (Fig. S2). Virtually all precipitation occurred during this period and precipitation estimates (13 to 23 mm) suggest that at higher elevations rainfall contributed a larger proportion (e.g. 18 to 32% at M140) to the runoff than at lower elevations. The highest daily precipitation totals on 27 August (8.4 mm in Kangerlussuaq and 3.9 mm at M0) were coincident with the highest daily total melt (e.g. 53 mm w.e. at M13), and a

transient excursion of the freezing level from ~1000 m asl to 2450 m asl, which is ~900 m above the long term ELA (Fig. S2c).

Due to the ice sheet's hypsometry the surface area that receives precipitation as rain and is exposed to melt increases non-linearly with a rising freezing level (Fig. 1b). We attribute the extremely high freezing level on 27 August (Fig. S2), which indicates melt and rainfall occurred up to 280 km inland, to the advection of warm, moist air over the GrIS from the southwest (Fig. 4). As a saturated air mass rises its cooling rate decreases due to the latent heat released by condensation. Accordingly, the lapse rate during the event was significantly lower (0.48° C / 100 m) than the annual mean (0.70° C / 100 m) and condensation at the ice surface resulted in an increased – and abnormally positive – latent heat flux that contributed 18% to the energy available for melting on 27 August (Fig. 3a). Melting consequently extended well into the accumulation area and across almost a third of the entire GrIS on this day[19].

Crucially, the event occurred in late summer when buffering of surface runoff in snowpack and firn was at an annual minimum. The decadal-high, end-of-season snowline (1696 m asl) exposed a large expanse of bare ice (Fig. 1b), and runoff during the event would have been efficiently concentrated into a mature network of channels and moulins developed during the preceding summer months, thereby facilitating rapid discharge into the subglacial environment. Nevertheless, total runoff during the late-August event was lower than mid-summer values when ice velocities were below the annual mean, inferring that runoff volume is not the only factor governing the acceleration we observe (Fig. 2). The seasonal evolution of subglacial drainage from an inefficient/distributed to an efficient system explains low mid-summer ice velocities at times of high melt input[7-12], and previous studies[20,21] argue that the antecedent subglacial

conditions modulate basal sliding. It is therefore significant that the event reported here occurred in late summer, immediately following a period of sub-zero air temperatures (Fig. 2a) and rapidly declining meltwater production: no melt was recorded at M61 for the week prior to the event (Fig. 2b). On 21 August, temperatures at the lowest-elevation AWS, M13, dropped below freezing for the first time since melt onset on 1 June resulting in the lowest daily melt rates, proglacial discharge and ice velocities since that date (Figs. 2 and 3). We interpret the gradual reduction in diurnal variability and simultaneous increase in borehole water pressure at R13 during the preceding period (Fig. 3) as evidence of a pre-event transition of the basal hydrological system to a less efficient winter-type mode[6,12]. The 3-day-lagged peak in proglacial discharge (Fig. 2c), of unprecedented magnitude in 2011 and which represents 13% of the annual total, supports this hypothesis as water transit is retarded under inefficient subglacial drainage conditions[22]. Hence, the late melt-season timing of the event critically dictated the ice sheet's dynamic response: the preceding week of sub-zero air temperatures (Fig. 2a) and declining melt (Figs. 2 and 3) primed the ice sheet for a high-magnitude flow response to this late-August runoff perturbation.

The rapid increase in subglacial water pressure recorded in two boreholes on Russell Glacier (at R13), as well those recorded on Isunngata Sermia[23] and Sermeq Avannarleq[6], to levels exceeding the ice overburden pressure suggest that the ice sheet was hydraulically decoupled from its bed during the acceleration event (Fig. 3c). This is confirmed by decimetre-scale surface uplift recorded at R13 (Fig. 3c) and at site A20 on Sermeq Avannarleq[6]. Uplift was sustained at R13 for ~ 22 hours before the surface lowered, returning to its pre-event height by 12:30 UTC on 3 September (Fig. 3c). Consistent with the theory of cavity opening[24], peak flow

acceleration was coincident with the highest rates of water pressure and uplift change, not their maxima. The sudden drop in water pressure and ice velocity on 31 August to levels lower than those prior to the acceleration event suggest the rapid post-event decline in surface runoff delivered a dramatically-reduced water flux to a drainage system with temporary over-capacity[12,21].

It is worth noting that rainfall events occurring earlier in the summer (e.g. 10 mm in Kangerlussuaq on 18 July) had no pronounced dynamic response (Fig. 2) as they did not challenge the capacity of what can be interpreted as an efficient subglacial drainage system at this time[7-12]. Importantly, the glaciological and meteorological conditions inherent to the late August event preferentially occur in late summer when the drainage system is closing down and cannot efficiently drain high runoff volumes. The advection of cyclonic weather systems over the GrIS is most frequent in August[25], and accordingly August is the wettest[15] and cloudiest[26] month in this region, with the heaviest rainfall (Fig. 5a) and peak net longwave radiation[26].

The spatial extent and frequency of these events

The acceleration event in late August 2011 provides a unique natural experiment to investigate the dynamic response of the GrIS to a spatially uniform and well-defined runoff perturbation. For eight days during late August and early September 2011, reanalysis data[27] indicate that a cyclone (minimum surface pressure of 992 hPa) centred on Baffin Bay off the west coast of Greenland advected warm, south-westerly airflow over the GrIS, bringing extensive precipitation, which was especially heavy in south-east Greenland (Figs. 4 and S9). These observations are consistent with lee-cyclogenesis whereby an Icelandic low-pressure system

forms in the lee of the GrIS off the southeast coast, while the parent cyclone delivers precipitation to west Greenland as it tracks north up the Davis Strait[28,29]. Occurring on 3.5% of all days between 1961-1999, and 6.3% of days in summer, Baffin Bay cyclones are the most frequent synoptic pattern that deliver precipitation to Greenland[29]. Reanalysis data confirm that the weather conditions driving the late-August acceleration prevailed across southern and western Greenland (Fig. 4).

We find that a concomitant flow response is evident in all available velocity records from these regions, including three major marine terminating glaciers located up to 370 km north of Kangerlussuaq: ice flow increased by 9% and 95% above the preceding week at GPS sites on Store Glacier[30] (S11) and Sermeq Avannarleq[6] (A20) respectively (Fig. 2d; Table S1). Repeat InSAR data[31] reveal that ice flow also increased by 10% on Jakobshavn Isbræ between 23 August and 3 September 2011 compared to 2-13 August (Fig. S3). The lower relative increase in ice velocity for the lower tongues of Store Glacier and Jakobshavn Isbræ (i.e. up to 10-15 km from the calving front) is not unexpected since it is well-established that the termini of fast marine-terminating glaciers experience smaller relative increases in velocity in response to surface water inputs compared to interior and land-terminating regions of the ice sheet that are remote from tidewater influences[32]. Simultaneous ice acceleration at all sites with contemporaneous data indicates that runoff during the late-August 2011 event overwhelmed the basal hydrological system of at least eight glaciers in southern and western Greenland (Figs. 1 and 2), including both land- and marine-terminating outlets. The acceleration in ice flow extended at least 140 km into the ice sheet interior (Fig. 2e), and we infer that this flow response was not just restricted to those sectors of the ice sheet with available velocity measurements.

This is the author's post-print. The final version was first published by Nature Geoscience on 13 July 2015, doi: 10.1038/NGEO2482

Moreover, three previous late-summer acceleration and uplift events identified on the GrIS in recent studies[14,33,34] can, with hindsight, now be re-interpreted as cyclonic rainfall/melt events (Fig. 5a). Previously, these pronounced acceleration events were interpreted as characteristic of late-summer melt-induced acceleration[14,33,34], which given their timing does not conform with the typical seasonal velocity cycle identified by subsequent studies[7-11]. Interrogation of reanalysis data and meteorological records (Figs. S4-7 and S10-12; Supplementary Section S1) reveal that these events were all driven by cyclonic conditions similar to those during late-August 2011. Many additional late-summer rainfall events are apparent from analysis of precipitation records (Fig. 5a), though unfortunately, velocity data are currently unavailable to determine the specific flow response to each of these perturbations.

Future impact on ice sheet mass balance and dynamics

Our findings lead us to the question of whether annual ice flow will increase in the future given predictions of a warmer, wetter climate. The delivery of surface water to the bed accelerates ice flow over the course of summer[14] yet recent studies[13,34-36] argue that annual ice flow in the ablation area is regulated by the melt-induced seasonal transition from inefficient/distributed to efficient subglacial drainage. Our observations support the hypothesis that high-magnitude inputs of water to the bed have the capacity to reorganise the basal drainage system, resulting in lower velocities following the event than preceded it[20,21,37]. It follows that, by establishing efficient subglacial drainage, such events will yield reduced post-event velocities and could therefore regulate ice flow over annual time scales[13,34-36,38]. While this self-regulation model appears to hold across the ablation area[13] and on Alaskan glaciers[38], where melt inputs to the basal drainage

This is the author's post-print. The final version was first published by Nature Geoscience on 13 July 2015, doi: 10.1038/NGEO2482

system are high and thin ice results in low basal conduit closure rates, this generalised model is unlikely to hold under a succession of late-season, cyclonic perturbations as described herein. Nor will flow within the interior of the GrIS self-regulate as thicker ice, lower net surface melt rates and shallower surface and bed slopes hinder the development of efficient subglacial drainage and its regulating influence[23,39,40]. Multi-year observations of increasing ice flow within the accumulation area of the GrIS[41] provide support for this latter premise. Furthermore, higher-order three-dimensional ice flow modelling[42] indicates that the net annual flow and discharge of the GrIS is indeed sensitive to and will increase in response to a greater frequency and spatial extent of high-magnitude runoff events anticipated under a warmer climate.

The advection of warm, moist air masses and rainfall over Greenland is predicted to become more frequent through the twenty-first century, in response to a warmer and cloudier regional climate and a northward shift in storm tracks[4,5,43-45]. Consistent with modelling experiments[43], analysis of Kangerlussuaq precipitation records and HIRHAM5 model simulations reveal that the seasonal distribution of rainfall has already increased over the last thirty years, with a tendency for a higher proportion of rain falling later in the season (Figs. 5 and S8) when the subglacial drainage system is likely to be highly sensitive to water inputs. A larger fraction of precipitation already falls as rain across the GrIS[46], and rain now falls at higher elevations (Fig. 5c) where the ice sheet is responsive to increased runoff[41]. Cyclonic-induced runoff events may therefore play a more prominent role in the mass balance and dynamics of the GrIS than they have previously, and their importance will increase if predicted changes in Greenland's climate[4,5,43-45,47] are realised.

This is the author's post-print. The final version was first published by Nature Geoscience on 13 July 2015, doi: 10.1038/NGEO2482

References:

1 Hanna, E. *et al.* Ice-sheet mass balance and climate change. *Nature* **498**, 51-59, doi:10.1038/nature12238 (2013).

2 Vaughan, D. G. *et al.* in *Climate Change 2013: The Physical Science Basis. Contribution of Working Group 1 to the Fifth Assessment Report of the Intergovernmental Panel on Climate Change* (Cambridge University Press, 2013).

3 van den Broeke, M. *et al.* Partitioning recent Greenland mass loss. *Science* **326**, 984-986, doi:10.1126/science.1178176 (2009).

4 Schuenemann, K. C. & Cassano, J. J. Changes in synoptic weather patterns and Greenland precipitation in the 20th and 21st centuries: 2. Analysis of 21st century atmospheric changes using self-organizing maps. *Journal of Geophysical Research* **115**, D05108, doi:10.1029/2009JD011706 (2010).

5 Vavrus, S. J. Extreme Arctic cyclones in CMIP5 historical simulations. *Geophysical Research Letters* **40**, 6208-6212, doi:10.1002/2013gl058161 (2013).

6 Andrews, L. C. *et al.* Direct observations of evolving subglacial drainage beneath the Greenland Ice Sheet. *Nature* **514**, 80-83, doi:10.1038/nature13796 (2014).

7 Bartholomew, I. *et al.* Seasonal evolution of subglacial drainage and acceleration in a Greenland outlet glacier. *Nature Geoscience* **3**, 408-411, doi:10.1038/Ngeo863 (2010).

8 Bartholomew, I. *et al.* Seasonal variations in Greenland Ice Sheet motion: Inland extent and behaviour at higher elevations. *Earth and Planetary Science Letters* **307**, 271-278, doi:10.1016/J.Epsl.2011.04.014 (2011).

9 Bartholomew, I. *et al.* Short-term variability in Greenland Ice Sheet motion forced by time-varying meltwater drainage: Implications for the relationship between subglacial drainage system behavior and ice velocity. *Journal of Geophysical Research* **117**, F03002, doi:10.1029/2011JF002220 (2012).

10 Colgan, W. *et al.* The annual glaciohydrology cycle in the ablation zone of the Greenland ice sheet: Part 1. Hydrology model. *Journal of Glaciology* **57**, 697-709, doi:10.3189/002214311797409668 (2011).

11 Hoffman, M. J., Catania, G. A., Neumann, T. A., Andrews, L. C. & Rumrill, J. A. Links between acceleration, melting, and supraglacial lake drainage of the western Greenland Ice Sheet. *Journal of Geophysical Research* **116**, F04035, doi:10.1029/2010JF001934 (2011).

12 Schoof, C. Ice-sheet acceleration driven by melt water supply variability. *Nature* **468**, 803-806, doi:10.1038/nature09618 (2010).

13 Sole, A. *et al.* Winter motion mediates dynamic response of the Greenland Ice Sheet to warmer summers. *Geophysical Research Letters* **40**, 3940-3944, doi:10.1002/grl.507764 (2013).

14 Zwally, J. H. *et al.* Surface melt-induced acceleration of Greenland ice-sheet flow. *Science* **297**, 218-222, doi:10.1126/science.1072708 (2002).

15 Cappelen, J., Jørgensen, B. V., Laursen, E. V., Stannius, L. S. & Thomsen, R. S. Technical Report 00-18: The observed climate of Greenland, 1958-99 - with climatological standard normals, 1961-90. Report No. 00-18 (Danish Meteorological Institute, Copenhagen). (2001). Accessed at: http://www.dmi.dk/fileadmin/user_upload/Rapporter/TR/2000/tr00-18.pdf on 13 April 2015.

16 Gascon, G., Sharp M. & Bush, A. Changes in melt season characteristics on Devon Ice Cap, Canada, and their association with the Arctic atmospheric circulation. *Annals of Glaciology* **54**, 101-110, doi:10.3189/2013AoG63A601 (2013).

17 van den Broeke, M. R., Smeets, C. J. J. P. & van de Wal, R. S. W. The seasonal cycle and interannual variability of surface energy balance and melt in the ablation zone of the west Greenland ice sheet. *The Cryosphere* **5**, 377-390, doi:10.5194/tc-5-377-2011 (2011).

18 van de Wal, R. S. W. *et al.* Twenty-one years of mass balance observations along the K-transect, West Greenland. *Earth System Science Data* **4**, 31-35, doi:10.5194/essdd-5-351-2012 (2012).

19 Mernild, S. H. & Liston, G. E. Surface melt extent for the Greenland Ice Sheet, 2011. *Geografisk Tidsskrift* **112**, 84-88 (2012).

20 Fudge, T. J., Harper, J. T., Humphrey, N. F. & Pfeffer, W. T. Rapid glacier sliding, reverse ice motion and subglacial water pressure during an autumn rainstorm. *Journal of Glaciology* **50**, 101-107, doi:10.3189/172756409789624247 (2009).

21 O'Neel, S., Echelmeyer, K. A. & Motyka, R. J. Short-term flow dynamics of a retreating tidewater glacier: LeConte Glacier, Alaska, U.S.A. *Journal of Glaciology* **47**, 567-578, doi:10.3189/172756503781830430 (2001).

22 Chandler, D. M. *et al.* Evolution of the subglacial drainage system beneath the Greenland Ice Sheet revealed by tracers. *Nature Geoscience* **6**, 195-198, doi:10.1038/Ngeo1737 (2013).

23 Meierbachtol, T., Harper, J. & Humphrey, N. Basal drainage system response to increasing surface melt on the Greenland ice sheet. *Science* **341**, 777-779, doi:10.1126/science.1235905 (2013).

24 Iken, A. The effect of the subglacial water pressure on the sliding velocity of a glacier in an idealized numerical model. *Journal of Glaciology* **27**, 407-421 (1981).

25 Serreze, M., Box, J., Barry, R. & Walsh, J. Characteristics of Arctic synoptic activity, 1952–1989. *Meteorology and Atmospheric Physics* **51**, 147-164, doi:10.1007/BF01030491 (1993).

26 van den Broeke, M., Smeets, P., Ettema, J. & Munneke, P. K. Surface radiation balance in the ablation zone of the west Greenland ice sheet. *Journal of Geophysical Research* **113**, D13105, doi:10.1029/2007JD009283 (2008).

27 Kalnay, E. *et al.* The NCEP/NCAR 40-year reanalysis project. *Bulletin of the American meteorological Society* **77**, 437-471, doi:10.1175/1520-0477(1996)077<0437:TNYRP>2.0.CO;2 (1996).

28 Chen, Q.-s., Bromwich, D. H. & Bai, L. Precipitation over Greenland retrieved by a dynamic method and its relation to cyclonic activity. *Journal of Climate* **10**, 839-870, doi:10.1175/1520-0442(1997)010<0839:POGRBA>2.0.CO;2 (1997).

29 Schuenemann, K. C., Cassano, J. J. & Finnis, J. Synoptic Forcing of Precipitation over Greenland: Climatology for 1961-99. *J Hydrometeorol* **10**, 60-78, doi:10.1175/2008jhm1014.1 (2009).

30 Ahlstrøm, A. P. *et al.* Seasonal velocities of eight major marine-terminating outlet glaciers of the Greenland ice sheet from continuous in situ GPS instruments. *Earth Syst. Sci. Data* **5**, 277-287, doi:10.5194/essd-5-277-2013 (2013).

31 Joughin, I., Smith, B., Howat, I. & Scambos, T. MEaSUREs Greenland Ice Velocity: Selected Glacier Site Velocity Maps from InSAR. Wcoast-69.10N (Updated in 2014) (Boulder, Colorado USA: NASA National Snow and Ice Data Center Distributed Active Archive Center. , 2011). Accessed at: http://dx.doi.org/10.5067/MEASURES/CRYOSPHERE/nsidc-0481.001. on 13 April 2015.

32 Joughin, I. *et al.* Seasonal speedup along the western flank of the Greenland Ice Sheet. *Science* **320**, 781-783, doi:10.1126/science.1153288 (2008).

33 Palmer, S., Shepherd, A., Nienow, P. & Joughin, I. Seasonal speedup of the Greenland Ice Sheet linked to routing of surface water. *Earth and Planetary Science Letters* **302**, 423-428, doi:10.1016/j.epsl.2010.12.037 (2011).

This is the author's post-print. The final version was first published by Nature Geoscience on 13 July 2015, doi: 10.1038/NGEO2482

34 van de Wal, R. S. W. *et al.* Large and rapid melt-induced velocity changes in the ablation zone of the Greenland Ice Sheet. *Science* **321**, 111-113, doi:10.1126/science.1158540 (2008).

35 Tedstone, A. J. *et al.* Greenland ice sheet motion insensitive to exceptional meltwater forcing. *Proceedings of the National Academy of Sciences*, doi:10.1073/pnas.1315843110 (2013).

36 van de Wal, R. S. W. *et al.* Self-regulation of ice flow varies across the ablation area in south-west Greenland. *The Cryosphere* **9**, 603-611, doi:10.5194/tc-9-603-2015 (2015).

37 Gudmundsson, G. H. *et al.* High-resolution measurements of spatial and temporal variations in surface velocities of Unteraargletscher, Bernese Alps, Switzerland. *Annals of Glaciology* **31**, 63-68, doi:10.3189/172756400781820156 (2000).

38 Burgess, E. W., Larsen, C. F. & Forster, R. R. Summer melt regulates winter glacier flow speeds throughout Alaska. *Geophysical Research Letters* **40**, 6160-6164, doi:10.1002/2013gl058228 (2013).

39 Dow, C. F., Kulessa, B., Rutt, I. C., Doyle, S., H. & Hubbard, A. Upper bounds on subglacial channel development for interior regions of the Greenland ice sheet. *Journal of Glaciology* **60**, 1044-1052, doi:10.3189/2014JoG14J093 (2014).

40 Dow, C. F. *et al.* Modeling of subglacial hydrological development following rapid supraglacial lake drainage. *Journal of Geophysical Research: Earth Surface*, 2014JF003333, doi:10.1002/2014jf003333 (2015).

41 Doyle, S. H. *et al.* Persistent flow acceleration within the interior of the Greenland ice sheet. *Geophysical Research Letters* **41**, 899-905, doi:10.1002/2013gl058933 (2014).

42 Bougamont, M. *et al.* Sensitive response of the Greenland Ice Sheet to surface melt drainage over a soft bed. *Nat Commun* **5**, doi:10.1038/Ncomms6052 (2014).

43 Bintanja, R. & Selten, F. M. Future increases in Arctic precipitation linked to local evaporation and sea-ice retreat. *Nature* **509**, 479-482, doi:10.1038/Nature13259 (2014).

44 Fettweis, X., Belleflamme, A., Erpicum, M., Franco, B. & Nicolay, S. Estimation of the sea level rise by 2100 resulting from changes in the surface mass balance of the Greenland ice sheet in *Climate Change: Geophysical Foundations and Ecological Effects* (eds J. Blanco & H. Kheradmand), 503-520 (2011).

45 Franco, B., Fettweis, X. & Erpicum, M. Future projections of the Greenland Ice Sheet energy balance driving the surface melt. *The Cryosphere* **7**, 1-18, doi:10.3189/2014JoG14J093 (2013).

46 Box, J. E. *et al.* Greenland ice sheet albedo feedback: thermodynamics and atmospheric drivers. *The Cryosphere* **6**, 821-839, doi:10.5194/Tc-6-821-2012 (2012).

47 Climate Change 2013: The Physical Science Basis. Contribution of Working Group I to the Fifth Assessment Report of the Intergovernmental Panel on Climate Change. (Cambridge University Press, Cambridge, United Kingdom and New York, 2013).

This is the author's post-print. The final version was first published by Nature Geoscience on 13 July 2015, doi: 10.1038/NGEO2482

Extended online methods

1. GPS measurements of ice surface motion

We used five dual-frequency Global Positioning System (GPS) receivers (R2, R13, I14, I27 and I46) capable of resolving three dimensional ice surface velocities at a high temporal resolution (< 1 hour), and three single-frequency GPS receivers (R38, R52, and R88) capable of resolving horizontal ice surface velocities at a daily time-step (Fig. 1).

Data from the dual-frequency receivers were processed kinematically[48] at a 30-second interval relative to bedrock-mounted reference stations using the carrier phase differential positioning software Track v. 1.24[49] and final precise ephemeris from the International GNSS Service[50]. Reference GPS stations were located 1 km from the terminus of Russell Glacier (BASE) and at Kellyville (KELY) giving baseline lengths of 5 to 46 km. Assuming steady ice motion, uncertainties in the positions were estimated at < 0.02 m in the horizontal and < 0.05 m in the vertical by examining the detrended position time series for GPS receiver R13 in early June 2011. High frequency noise was filtered with a two-pole, low-pass Butterworth filter with a 12-hour cut-off period. To reduce the effect of bed parallel motion the surface height record presented in Figure 3c was linearly detrended.

A sixth dual-frequency receiver was located at R140 (co-located with M140) but due to the low velocity at this site (~ 52 m yr^{-1}), which is located 50 km above the long-term mean equilibrium line, and the long baseline length (> 140 km) a different, more rigorous, processing strategy was used to process data from this site and the methods are detailed in Ref. 41.

This is the author's post-print. The final version was first published by Nature Geoscience on 13 July 2015, doi: 10.1038/NGEO2482

The single-frequency receivers recorded horizontal position every hour and the resulting time-series were filtered with a 48-hour-period average[51]. We did not attempt to resolve vertical motion from the single-frequency GPS records as the detection limit is close to the magnitude of ice surface uplift[51].

Daily averaged horizontal velocity was calculated by differencing the filtered positions at a daily time step. We calculated the annual velocity (Table S1) from positions of the antenna on 6 June 2010 and 6 June 2011 for Russell Glacier GPS and from 2 September 2011 and 2 September 2012 for Isunngata Sermia GPS. These dates were selected on the basis of available data and to avoid times when antenna poles were relocated (e.g. 7 June 2011 for GPS R13 and R2).

To investigate whether ice flow acceleration occurred in other regions of the GrIS during the late August / September 2011 event, we examined all available GPS records from published studies. Flow acceleration was evident in all available records with contemporaneous data, and these records are presented in Figure 2d as daily-averaged speed above the annual mean. These data from sites S11 and A20 are from Store Glacier and Sermeq Avannarleq and are adapted from Refs. 30 and 6 respectively. S11 consisted of an L1 GPS receiver located 11 km from the calving front of marine-terminating Store Glacier[30] and A20 consisted of a dual-frequency GPS receiver located at the FOXX borehole and automated weather station (AWS) site[6], ~20 km from the terminus of marine-terminating Sermeq Avannarleq (Table S1), which is ~ 26 km down-glacier of Swiss Camp[14]. S11 flows an order of magnitude faster than all the other GPS sites in Figure 2d owing to its proximity to the calving front of this fast marine-terminating outlet glacier. The seasonal velocity cycle at S11 is also markedly different and can be explained by the

influence of sea ice melange[52]. The magnitude and seasonal variation in velocity at A20 is, on the other hand entirely consistent with the sites on Russell Glacier and Isunngata Sermia (Fig. 2d).

2. TanDEM-X methods & verification against GPS records

We applied offset tracking on repeat pass TanDEM-X data to derive surface velocities for the ice sheet margin in August and September 2011. TanDEM-X (TerraSAR-X add-on for Digital Elevation Measurement) is a bi-static Synthetic Aperture Radar (SAR) mission launched in June 2010 with the two satellites orbiting in a closely controlled formation with typical distances between 250 and 500 m. The satellites circle on an 11-day repeat orbit, acquiring SAR images, with a 30 x 50 km footprint, at a 3 m spatial resolution[53].

We used three ascending images acquired on 1 August, 23 August, and 3 September 2011. We combined the first two acquisitions (1 August, 23 August; 22 days separation) in order to derive the 'average August' ice velocities, and the images recorded on 23 August and 03 September (11-day separation) for detecting the late August acceleration (Fig. S1). We computed SAR amplitude images for each of the scenes and applied an image-to-image cross-correlation technique to track the motion of features on the glacier surface[54].

The accuracy of the derived flow speeds was investigated by a comparison with velocities for the same time intervals at two GPS locations: R2 and R13 (see inset on Figure S1). We found good agreement for both periods, with differences ranging between 0.011 m d^{-1} (R2, 1 to 23 August) and 0.058 m d^{-1} (R13, 23 August to 3 September).

In addition to the TanDEM-X measurements described above for the Kangerlussuaq sector, InSAR speed differences across the Jakobshavn Isbræ catchment were calculated from velocity

maps derived from TerraSAR-X image pairs[31] for a pre-event period (2 to 13 August 2011) and a period representing the event (23 August to 3 September 2011), see Figure S3. Potential control-related errors along the ice-sheet margin are presumed small (<10 m a^{-1}) relative to variations in ice-flow speed, although height errors in the digital elevation model used for topographic correction in the original processing can yield absolute errors of up to ~3% of speed[55].

3. Borehole water pressure

We present data from a wired pressure sensor installed 0.5 m from the ice-bed interface at site R13/M13, and express borehole water pressure as a percentage of the ice overburden pressure assuming an ice thickness of 610 m and a density of ice of 917 kg m^{-3} (Fig. 3c). Further description of the methods used to drill and instrument the borehole is detailed in a previous study[56].

4. Meteorological measurements

Meteorological measurements were made by three on-ice AWS located 13 km (M13), 61 km (M61) and 140 km (M140) from the terminus of Russell Glacier, and one on-tundra AWS (M0) located 1 km west of the ice margin (Fig. 1, Table S2). To keep consistency with the GPS site names, the numbers in the AWS site labels refer to the distance from the terminus of Russell Glacier. The on-ice AWS were previously referred to as KAN_L (M13; co-located with R13), KAN_M (M61) and KAN_U (M140; co-located with R140), and we direct the reader to Ref. 57 for further information on the AWS methods. The AWS recorded surface height change due to accumulation and ablation, air pressure, temperature and humidity, wind speed and direction, and downward and upward shortwave and longwave radiation at 2-3 m above the surface. The AWS sampled at a 10-minute interval, from which hourly averages were calculated. The energy

This is the author's post-print. The final version was first published by Nature Geoscience on 13 July 2015, doi: 10.1038/NGEO2482

available for melt was determined using a surface energy balance model[58], validated using the AWS measurements of surface temperature and surface height change[57].

4.1. Estimating cloud cover and the freezing level

Cloud cover was approximated making use of the strong dependence of downwards longwave radiation on atmospheric moisture[58]. A full cloud cover was assumed for high downward longwave radiation values at a certain air temperature, clear skies for low values, with a linear transition for values in between. We estimated the elevation of the freezing level using lapse rates calculated from M61 and M140 air temperature measurements.

4.2. Precipitation measurements

Precipitation records from site M0 and Kangerlussuaq (DMI station 04231)[59] were corrected for wind and adhesion loss effects, using site-specific correction factors[60,61]. We applied correction factors of 33% for snow and 16% for rain for the automatic GEONOR gauge deployed < 1 km from the ice margin at M0, a site that is exposed to the wind. For the manual gauge at Kangerlussuaq, which is more sheltered from the wind, we applied correction factors of 12% for snow and 4.5% for rain. At both sites the adhesion loss was set to 0.1 mm per precipitation event, and mass loss due to evaporation was assumed to be zero.

4.3. Decomposing the surface energy budget

We gained further insight into the abnormal runoff caused by this weather event by decomposing the surface energy budget (SEB) for the AWS at site M13 (Fig. 3a) on Russell Glacier. The net shortwave (SW_{net}) and net longwave (LW_{net}) radiation, the sensible (SHF) and latent (LHF) heat fluxes, and the ground flux (GF) are defined as positive when they add heat to the surface.

This is the author's post-print. The final version was first published by Nature Geoscience on 13 July 2015, doi: 10.1038/NGEO2482

Although clouds reduce net shortwave radiation, through the so called longwave cloud-effect they can increase LW_{net} as a larger fraction of the outgoing longwave radiation is absorbed by clouds and re-radiated back to the surface[17,62]. LW_{net} typically represents a heat sink in the SEB but under certain atmospheric conditions[16,63] it can be positive resulting in higher net radiation ($R_{net} = SW_{net} + LW_{net}$) than under clear skies. Accordingly, although daily total SW_{net} on 27 August was less than half (4.9 MJ m^{-2} day^{-1}) than that recorded under clear sky conditions seven days previously on 21 August (10.3 MJ m^{-2} day^{-1}), net radiation was greater on the 27 August (5.2 MJ m^{-2} day^{-1}) compared to 21 August (4.5 MJ m^{-2} day^{-1}) owing largely to the LW_{net} being positive (Fig. 3a). The largest energy source during the event was, however, the sensible heat flux (SHF) which accounted for more than 50% of the surface energy budget between 26 to 28 August – a marked increase on the pre-event values (e.g. 19% on 21 August 2011) under clear skies (Fig. S2a) and with low wind speeds (Fig. S2b). The increase in SHF can be attributed to the high near-surface temperature resulting from the advection of warm air over the ice sheet (Fig. 4). Moisture condensation onto the ice surface due to high specific humidity and wind speed resulted in a positive latent heat flux (LHF; e.g. 3.0 MJ m^{-2} day^{-1}, or 18% of the SEB on 27 August), as opposed to surface evaporative cooling (e.g. −0.73 MJ m^{-2} day^{-1} on 21 August), which is more frequent under the prevalent clear sky conditions (Fig. 3a). Both turbulent heat fluxes (SHF and LHF) are enhanced by high wind speeds (e.g. 8 m s^{-1} on 27 August; Fig. S2b), which increase the vertical mixing of air[17,64].

For a given air temperature, moist conditions have lower lapse rates and therefore higher freezing levels than dry conditions. The lapse rate during the late August event (24 to 31 August) was much lower (0.48° C/100 m) than the annual mean (0.70° C/100 m), resulting in the 0° C

isotherm attaining an exceptionally high elevation of ~ 2450 m asl on 27 August 2011. Air temperatures at M61 (1280 m asl) were continuously above freezing during the late August event (Fig. 2a). Even at M140, ~ 50 km inland from the mean 1990-2011 equilibrium line, positive air temperatures suggest precipitation was liquid at least 140 km inland (Fig. S2c).

The surface energy balance model does not account for the heat delivered by rain, which we found was minimal. The heat flux of rain Q_R is given by:

$$Q_R = \rho_w C_w R(T_r - T_s) \quad \text{Eq. 1}$$

where ρ_w is the density of water, C_w is the specific heat capacity of water (4.2 kJ kg^{-1} K^{-1}), R is the rainfall rate, and T_r and T_s are the temperatures of rain and the surface respectively[65]. Given a surface temperature of a melting ice surface of 0° C, a rain temperature of 6° C, and the lower (15 mm) and upper (24mm) estimates of rainfall during the event we estimate that the rain heat flux contributed 0.06 to 0.1 MJ m^{-2} day^{-1}. This is equivalent to 1.1 to 1.8 mm w.e. of rain-induced ice melt during the entire event, which represents a small component of the runoff during the event (e.g. 0.5 % at M13).

At higher elevations the sensible and latent heat released by rainfall cooling and freezing in a surface snowpack may, however, have played an important role in bringing the sub-freezing snowpack to the melting point. The energy flux Q_R supplied by rain freezing in a snowpack is given by:

$$Q_R = \rho_w C_s R(T_r - T_s) + \rho_w \lambda_w R, \quad \text{Eq. 2}$$

where C_s is the specific heat capacity of snow (2090 J Kg^{-1} K^{-1}), and λ_w is the latent heat of fusion (334 kJ Kg^{-1}). The rain temperature of 2° C is taken to be the air temperature at M140

during the rainfall event and the temperature of the snowpack of −15° C is based on the mean air temperature during the preceding week. Given these estimates, 14 mm of rain at 2° C would bring a 15 cm w.e. snowpack at −15° C to the melting point. Hence, the energy released by rain cooling and freezing is a very effective heating mechanism for sub-freezing snowpacks and this will have enhanced melt rates at high elevations.

All these energy sources – an abnormally positive net longwave radiation, the sensible heat flux, the latent heat flux from condensation and the rain heat flux – contributed to high melt conditions peaking on 27 August, coincident (Fig. 2b) with the highest precipitation (Fig. 2a,b), wind speeds (Fig. S2b), and freezing level (Fig. S2c), which combined to produce abnormally high-magnitude runoff for this time of year (Fig. 2).

4.4. Calculating the elevation of the snowline

The elevation of the snowline – the maximum elevation that snow remains at the end of the melt season – was retrieved from end-of-melt-season visible-band Moderate Resolution Imaging Spectrometer (MODIS) images[66]. The ice-sheet-wide, MODIS-retrieved snowlines, which are calibrated against the K-transect surface mass balance observations[18], are available at http://bprc.osu.edu/wiki/Greenland_Ice_Sheet_Snowline.

5. Reanalysis

We used data from the National Centers for Environmental Prediction/National Centre for Atmospheric Research (NCEP/NCAR) reanalysis project[27] to track weather systems, and to estimate precipitation and the near surface air temperature anomaly over Greenland (Figs. 4, S4-6 and S9-12). These reanalysis data reveal that a low-pressure system (minimum surface pressure of 992 hPa) tracking across Baffin Bay between 24 to 30 August 2011 caused warm south-

westerly airflow (Fig. 4), which resulted in cloud-cover (Fig. S2a) and precipitation (Fig. 4) over southern and western Greenland. Such Baffin Bay cyclones are the most frequent synoptic pattern that bring precipitation to Greenland[29]. They often bifurcate over the southern GrIS forming an Icelandic Low by lee-cyclogenesis on the southeast coast, while the parent cyclone tracks north delivering precipitation to the west coast of Greenland[28,29]. They advect warm moist air onshore from the open North Atlantic, which is lifted orographically over the ice sheet to an elevation of 2800 m above sea level in less than 200 km[29]. As the air rises, it cools adiabatically becoming saturated and releasing precipitation. Baffin Bay cyclones occur more frequently during the summer (6.35% of days) than during winter (2.90% of days)[29] and atmospheric models[4] predict that they will increase in frequency from 3% of days in 1961-99 to 4% of days in 2081-2100. The widespread nature of the precipitation and heat delivered by the August-September 2011 event is demonstrated by the reanalysis data (Figs. 4 and S9) and acceleration in ice flow is evident in all available velocity records from southern and western Greenland during this period (Figs. 1, 2d and S3). Substantial acceleration was measured on three major marine-terminating glaciers in West Greenland, including Sermeq Avannarleq[6], Store Glacier[30] and Jakobshavn Isbræ (Figs. 2d and S3).

6. Investigating long-term trends in rainfall seasonality

To investigate changes in the seasonal distribution of rainfall over the last two to three decades we examined long-term trends in the Kangerlussuaq precipitation record[59] between 1977 and 2012. The phase of precipitation was determined as liquid if the mean temperature over the corresponding 12-hour period was greater than or equal to 2° C, allowing daily total rainfall to be calculated.

This is the author's post-print. The final version was first published by Nature Geoscience on 13 July 2015, doi: 10.1038/NGEO2482

Following standard statistical measures applied by previous studies[67,68] we calculated the seasonality index (SI) and the day of year on which the 10th (P10), 25th (P25), 50th (P50), 75th (P75) and 90th (P90) percentiles of the annual total rainfall were achieved. We assessed the dispersion in the seasonal distribution of rainfall by calculating the interquartile $(IQR = P75 - P25)$ and interdecile range $(IDR = P90 - P10)$. The seasonality index (SI):

$$SI = \frac{1}{R}\sum_{n=1}^{12}\left|\overline{X}_n - \frac{R}{12}\right| \qquad \text{Eq. 3}$$

where R is the total annual rainfall and $\overline{X}$ is the total monthly rainfall in month n, is a standard measure of rainfall seasonality[68]. SI theoretically ranges from 0, if all the months have equal rainfall to 1.83, if all the rainfall falls in one month. SI values of 1 to 1.19 indicate that the majority of rainfall occurs in 3 months or less with SI > 1.2 indicating the majority of rainfall falls in 2 months or less.

We investigated the timing of heavy rainfall events by calculating the fortnightly totals of rainfall for the entire Kangerlussuaq precipitation record. To normalise the influence of exceptional events between years, we divided fortnightly precipitations sums by their respective annual total (Fig. 5a). Heavy rainfall events, identified as dark red blocks on Figure 5a, tend to occur more frequently in late summer and early autumn, coinciding with the period of highest rainfall[15], peak longwave radiation, densest cloud cover[17] and peak cyclonic activity[25] in this region.

7. HIRHAM5 Methods

We examined changes in rainfall across the K-transect[18] over the last two decades using the HIRHAM5 regional climate model (RCM)[69]. The HIRHAM5 RCM is driven at the lateral

boundaries by the ERA-Interim reanalysis[70] and provides estimates of solid and liquid precipitation at 5 km horizontal resolution. The simulations are validated against observations from meteorological stations on the land[59] and AWS on the ice sheet[57,71]. Generally, the temperature and precipitation biases are small, indicating a realistic simulation of the climate over Greenland[72]. We averaged the rain fraction estimated by the HIRHAM5 RCM over two periods (1990 – 1999 and 2000 – 2009) at each grid cell along the K-transect at a weekly time step (Fig. 5c).

References for extended online methods:

48 King, M. Rigorous GPS data-processing strategies for glaciological applications. *Journal of Glaciology* **50**, 601-607, doi:10.3189/172756504781829747 (2004).

49 Chen, G. *GPS kinematic positioning for the airborne laser altimetry at Long Valley, California*, Mass. Inst. of Technol., Cambridge, (1998).

50 Dow, J. M., Neilan, R. E. & Rizos, C. The International GNSS Service in a changing landscape of Global Navigation Satellite Systems. *Journal of Geodesy* **83**, 191-198, doi:10.1007/s00190-008-0300-3 (2009).

51 Den Ouden, M. A. G. *et al.* Stand-alone single-frequency GPS ice velocity observations on Nordenskioldbreen, Svalbard. *The Cryosphere* **4**, 593-604, doi:10.5194/tc-4-593-2010 (2010).

52 Walter, J. I. *et al.* Oceanic mechanical forcing of a marine-terminating Greenland glacier. *Annals of Glaciology* **53**, 181-192, doi:10.3189/2012AoG60A083 (2012).

53 Krieger, G. *et al.* TanDEM-X: A satellite formation for high-resolution SAR interferometry. *Geoscience and Remote Sensing, IEEE Transactions on* **45**, 3317-3341, doi:10.1109/TGRS.2007.900693 (2007).

54 Strozzi, T., Luckman, A., Murray, T., Wegmuller, U. & Werner, C. L. Glacier motion estimation using SAR offset-tracking procedures. *Geoscience and Remote Sensing, IEEE Transactions on* **40**, 2384-2391, doi:10.1109/TGRS.2002.805079 (2002).

55 Joughin, I., Smith, B. E., Howat, I. M., Scambos, T. & Moon, T. Greenland flow variability from ice-sheet-wide velocity mapping. *Journal of Glaciology* **56**, 415-430, doi:10.3189/002214310792447734 (2010).

56 Smeets, C. J. P. P. *et al.* Instruments and Methods - A wireless subglacial probe for deep ice applications. *Journal of Glaciology* **58**, 841-848, doi:10.3189/2012JoG11J130 (2012).

57 van As, D. *et al.* Large surface meltwater discharge from the Kangerlussuaq sector of the Greenland ice sheet during the record-warm year 2010 explained by detailed energy balance observations. *The Cryosphere* **6**, 199-209, doi:10.5194/tc-6-199-2012 (2012).

58 van As, D. Warming, glacier melt and surface energy budget from weather station observations in the Melville Bay region of northwest Greenland. *Journal of Glaciology* **57**, 208-220, doi:10.3189/002214311796405898 (2011).

This is the author's post-print. The final version was first published by Nature Geoscience on 13 July 2015, doi: 10.1038/NGEO2482

59 Cappelen, J. *et al.* Technical Report 13-11: Weather observations from Greenland 1958-2012. (Danish Meteorological Institute, Copenhagen, 2013). Accessed at http://www.dmi.dk/fileadmin/Rapporter/TR/tr13-11.pdf on 9 June 2015.

60 Alexandersson, H. Korrektion av nederbord enligt enkel klimatologisk metodik. SMHI, Meteorologi, Nr 111. (2003).

61 Johansson, E. *et al.* Hydrological and meteorological investigations in a periglacial lake catchment near Kangerlussuaq, west Greenland – presentation of a new multi-parameter dataset. *Earth Syst. Sci. Data* **7**, 93-108, doi:10.5194/essd-7-93-2015 (2015).

62 Ambach, W. The influence of cloudiness on the net radiation balance of a snow surface with high albedo. *Journal of Glaciology* **13**, 73-84 (1974).

63 Bennartz, R. *et al.* July 2012 Greenland melt extent enhanced by low-level liquid clouds. *Nature* **496**, 83-86, doi:10.1038/nature12002 (2013).

64 van den Broeke, M. *et al.* Partitioning of melt energy and meltwater fluxes in the ablation zone of the west Greenland ice sheet. *The Cryosphere* **2**, 179-189, doi:10.5194/tc-2-179-2008 (2008).

65 Hock, R. Glacier melt: a review of processes and their modelling. *Progress in Physical Geography* **29**, 362-391, doi: 10.1191/0309133305pp453ra (2005).

66 Box, J. E., Benson, R. J., Decker, D. & Bromwich, D. H. Greenland ice sheet snow line variations, *Association of American Geographers Annual Meeting,* Las Vegas, NV, 22-28 March 2009 (2009).

67 Pryor, S. C. & Schoof, J. T. Changes in the seasonality of precipitation over the contiguous USA. *Journal of Geophysical Research* **113**, doi:10.1029/2008JD010251 (2008).

68 Walsh, R. P. D. & Lawler, D. M. Rainfall seasonality: description, spatial patterns and change through time. *Weather* **36**, 201-208, doi:10.1002/j.1477-8696.1981.tb05400.x (1981).

69 Christensen, O. B. *et al.* Tehnical Report 06-17: The HIRHAM regional climate model, version 5. (Danish Meteorological Institute, Copenhagen, 2006). Accessed at http://www.dmi.dk/fileadmin/Rapporter/TR/tr06-17.pdf on 13 April 2015.

70 Dee, D. P. *et al.* The ERA-Interim reanalysis: configuration and performance of the data assimilation system. *Quarterly Journal of the Royal Meteorological Society* **137**, 553-597, doi:10.1002/qj.828 (2011).

71 van de Wal, R. S. W., Greurell, W., van den Broeke, M. R., Reijmer, C. H. & Oerlemans, J. Surface mass-balance observations and automatic weather station data along a transect near Kangerlussuaq, West Greenland. *Annals of Glaciology* **42**, 311-316, doi:10.3189/172756405781812529 (2005).

72 Lucas-Picher, P. *et al.* Very high resolution regional climate model simulations over Greenland: Identifying added value. *Journal of Geophysical Research* **117**, doi:10.1029/2011JD016267. (2012).

This is the author's post-print. The final version was first published by Nature Geoscience on 13 July 2015, doi: 10.1038/NGEO2482

Acknowledgments

This research was funded by: SKB/Posiva through the Greenland Analogue Project (GAP); UK National Environment Research Council (NERC) grants NE/G005796/1, NE/G010595/1, NE/H024204/1; a Royal Geographical Society Gilchrist Fieldwork Award; and The Netherlands Organisation for Scientific Research (NOW/PPP) – the latter of which generously supported the K-transect measurements. TanDEM-X data were provided by the German Aerospace centre (DLR) within the framework of the XTI_GLAC0433 project. We thank UNAVCO, the National Snow and Ice Data Center, the Danish Meteorological Institute, MIT, John Cappellen, Rickard Pettersson, Katrin Lindback, and Andrew Fitzpatrick for help with data collection and processing. The crew of S/V Gambo are thanked for help in the deployment of the Store Glacier GPS. A.H. and H.P. were supported at the Centre for Arctic Gas Hydrate, Environment and Climate by funding from the Research Council of Norway (Grant No. 223259). S.H.D. was supported by an Aberystwyth University doctoral scholarship and NERC grant NE/K006126.

Author contributions

A.H., S.D., T.M., and J.H. collected the dual-frequency GPS data. S.D. processed the dual-frequency GPS data, collated the datasets, prepared the figures and wrote the original manuscript. R.W. and C.S. provided the single-frequency GPS data, whom together with F.W. acquired the borehole water pressure record. J.B. provided and interpreted the reanalysis data and advised on meteorology. D.A. collected and processed the AWS datasets and modelled the surface energy balance. K.S. processed the TanDEM-X datasets. E.J. applied the correction to the precipitation records. R.M. performed the HIRHAM5 regional climate modelling. B.H. advised on the analysis of borehole water pressure records and their relationship to ice velocity.

This is the author's post-print. The final version was first published by Nature Geoscience on 13 July 2015, doi: 10.1038/NGEO2482

H.P. processed the Terra SAR-X data for Jakobshavn Isbræ. P.C. and A.M. provided additional advice on data interpretation and analysis. All authors contributed to the subsequent editing of the manuscript. A.H. was the P.I. of the main project that conceived the study and co-developed it with S.D.

Author information

Correspondence and requests for materials should be addressed to Samuel Doyle (sdd08@aber.ac.uk). The authors declare no competing financial interests.

Supplementary information

Supplementary information is provided as a separate file.

This is the author's post-print. The final version was first published by Nature Geoscience on 13 July 2015, doi: 10.1038/NGEO2482

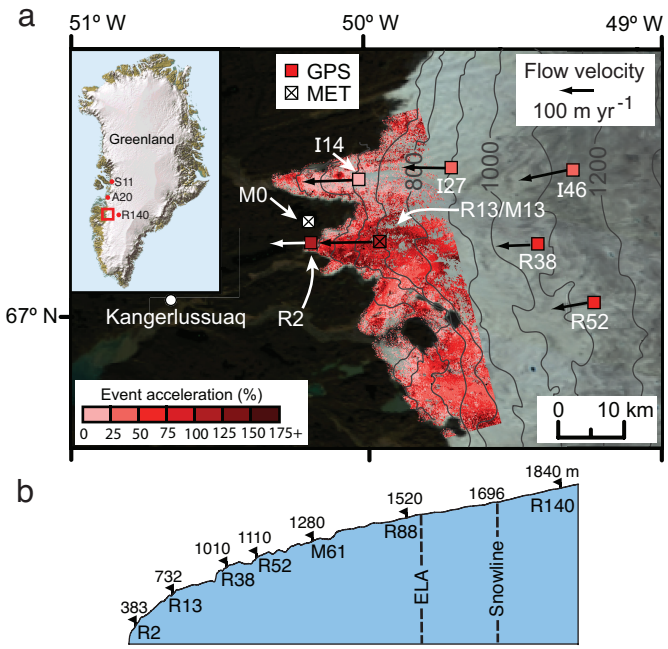

Fig. 1. (a) Map of the lower ablation area of the Kangerlussuaq sector. The background MODIS image was acquired on 17 August 2011. Acceleration during the late-August event (23 August – 3 September 2011) relative to the preceding period (1 – 23 Aug 2011) was derived from TanDEM-X velocity maps. The GPS symbol colours represent the percentage acceleration during the event (Table S1). The velocity vector shows the mean velocity during the late-August acceleration. The red box on the inset map shows the location in Greenland. **(b)** Russell Glacier's elevation profile with the ELA and snowline marked.

This is the author's post-print. The final version was first published by Nature Geoscience on 13 July 2015, doi: 10.1038/NGEO2482

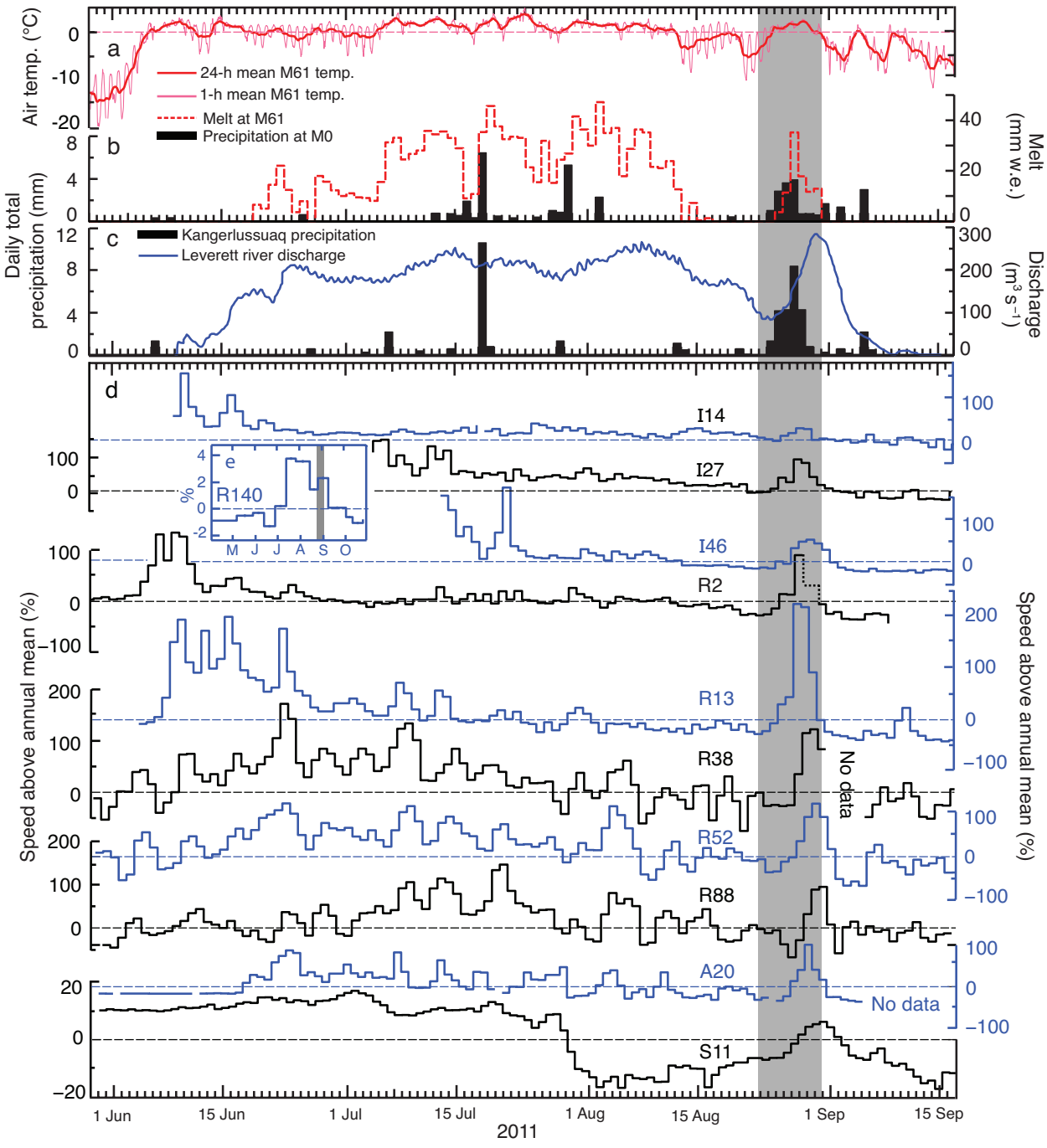

Fig. 2. Records of meteorology, proglacial discharge, and ice velocity for the 2011 melt season. (**a)** air temperature at M61 with a 1- and 24-hour average applied, **(b)** daily total melt at

This is the author's post-print. The final version was first published by Nature Geoscience on 13 July 2015, doi: 10.1038/NGEO2482

M61 and precipitation at M0, **(c)** precipitation in Kangerlussuaq and proglacial Leverett River discharge[13], **(d,e)** daily-averaged velocity at 11 GPS sites on land-terminating Russell (R) Glacier and Isunngata Sermia (I) and marine-terminating Store Glacier[30], (S) and Sermeq Avannarleq[6] (A), expressed as speed above the annual mean. Note the different y-axis scaling for S11 and R140. The timing of the late-August acceleration is shaded in grey.

This is the author's post-print. The final version was first published by Nature Geoscience on 13 July 2015, doi: 10.1038/NGEO2482

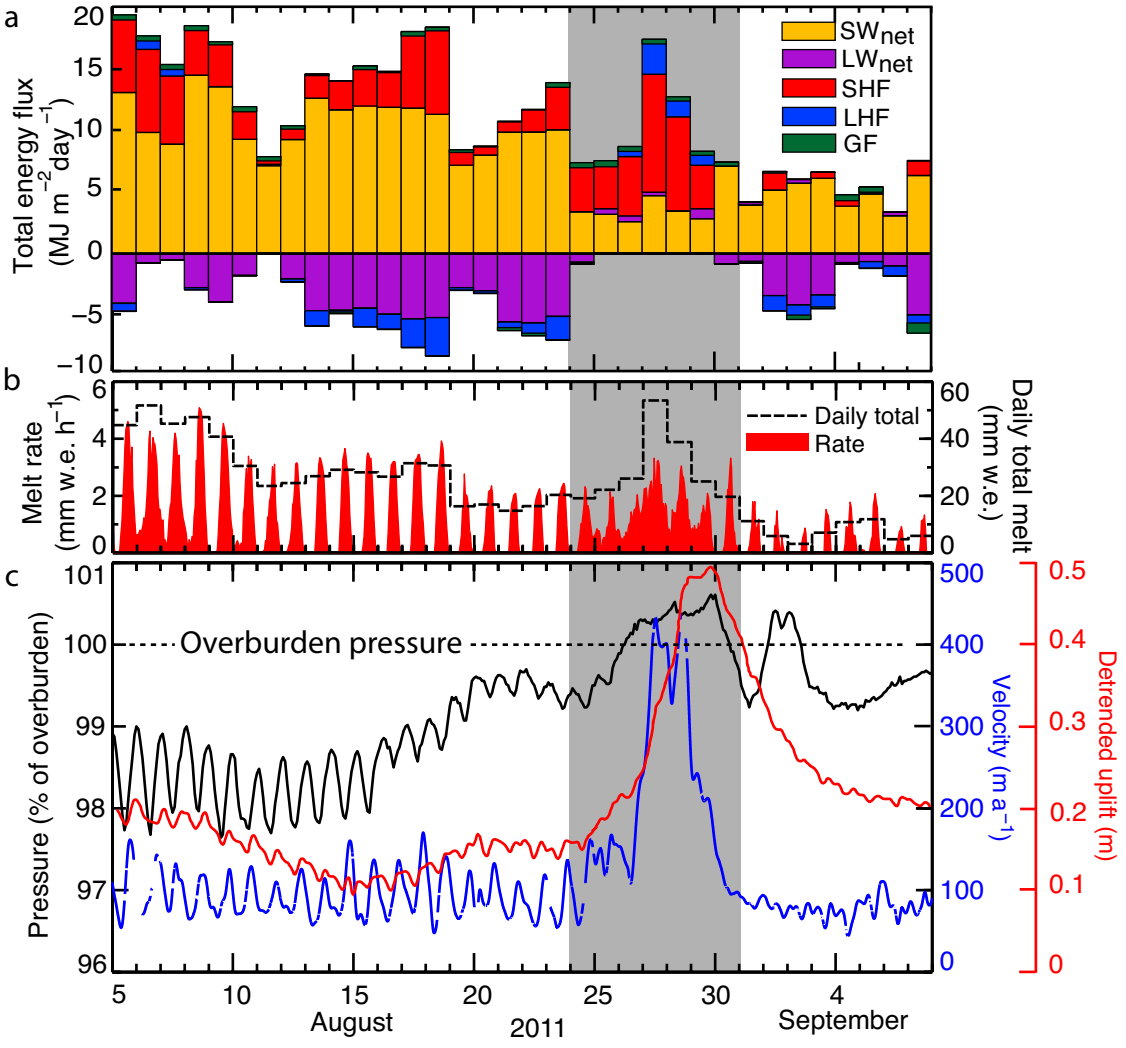

Fig. 3. The surface energy budget, melt, borehole water pressure and ice surface velocity and uplift at R13 (a) the surface energy budget at M13 at a daily time step. The components: net shortwave (SW_{net}) and net longwave (LW_{net}) radiation, the sensible (SHF) and latent (LHF) heat fluxes and the ground flux (GF) are defined as positive when they add heat to the surface. **(b)** Borehole water pressure, velocity, uplift and **(c)** melt at the R13 site. The timing of the late-August acceleration is shaded in grey.

This is the author's post-print. The final version was first published by Nature Geoscience on 13 July 2015, doi: 10.1038/NGEO2482

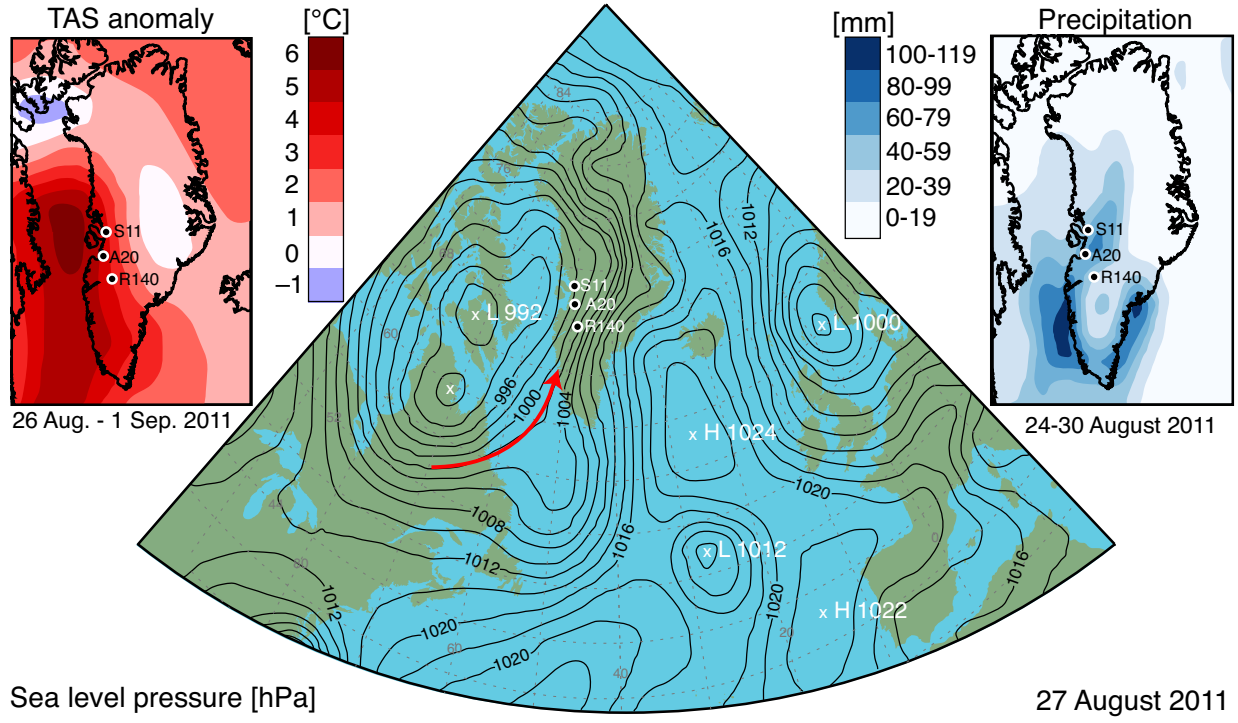

Fig. 4. Reanalysis data[27] for the August/September 2011 event including sea level pressure for 27 August 2011, the near surface air temperature (TAS) anomaly for the period 26 August to 1 September versus the same period in the 1981-2010 baseline, and total precipitation for the week 26-30 August. The red arrow indicates the direction of warm air advection.

This is the author's post-print. The final version was first published by Nature Geoscience on 13 July 2015, doi: 10.1038/NGEO2482

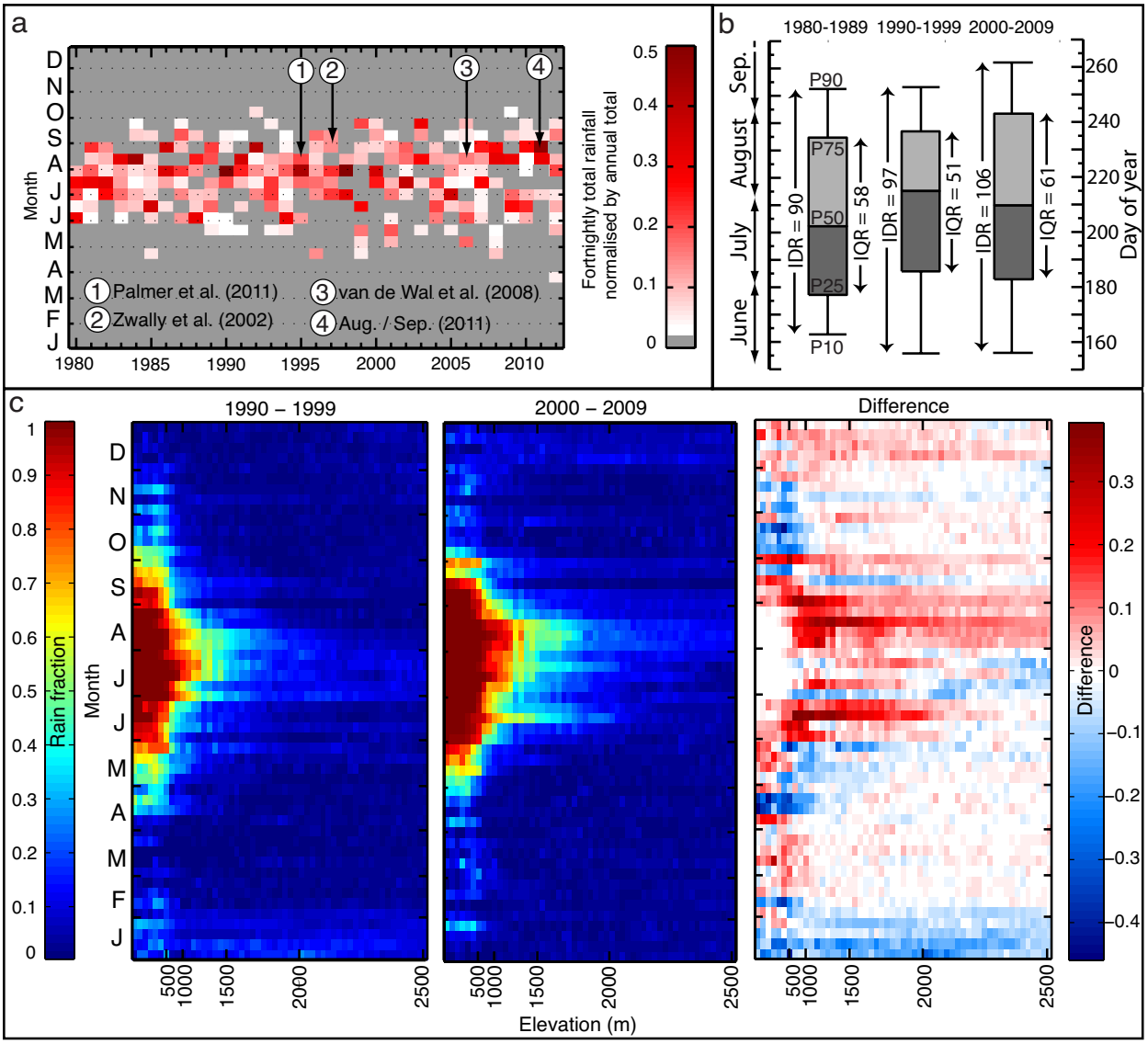

Fig. 5. Long term trends in rainfall seasonality and elevation. (a) fortnightly total rainfall in Kangerlussuaq normalised by the annual total between 1980 and 2012. Arrows indicate the 2011 event and three events evident in recent studies[14,33,34], **(b)** the decadal mean day of year on which the percentiles in total annual rainfall in Kangerlussuaq were achieved, and **(c)** HIRHAM5

regional climate model simulations of the rain fraction across the K-transect at a weekly time step. Heavy rainfall events appear on (a) as dark red blocks. The interquartile (IQR) and interdecile (IDR) ranges with units of days are annotated on (b).

This is the author's post-print. The final version was first published by Nature Geoscience on 13 July 2015, doi: 10.1038/NGEO2482

Supplementary information for "Amplified melt and flow of the Greenland ice sheet driven by late-summer cyclonic rainfall"

Samuel H. Doyle[1*], Alun L. Hubbard[2,1], Roderik S.W. van de Wal[3], Jason E. Box[4,5], Dirk van As[4], Kilian Scharrer[6], Toby W. Meierbachtol[7], Paul C.J.P. Smeets[3], Joel T. Harper[7], Emma Johansson[8,9], Ruth H. Mottram[10], Andreas B. Mikkelsen[11], Frank Wilhelms[12,13], Henry Patton[2], Poul Christoffersen[14], and Bryn Hubbard[1]

[1]Centre for Glaciology, Department of Geography & Earth Sciences, Aberystwyth University, Aberystwyth, SY23 3DB, UK.
[2] Centre for Arctic Gas Hydrate, Environment and Climate, Department of Geology, The Arctic University of Norway, Tromsø, Norway
[3]Institute for Marine and Atmospheric research Utrecht, Utrecht University, P.O. Box 80005, 3508TA Utrecht, Netherlands.
[4]Geological Survey of Denmark and Greenland, Øster Voldgade 10, 1350 Copenhagen K, Denmark.
[5]Department of Geography, The Ohio State University, 1036 Derby Hall, 154 North Oval Mall, Columbus, Ohio, 43210-1361, USA.
[6]ENVEO IT GmbH, Innsbruck, Austria.
[7]Department of Geosciences, University of Montana, Missoula, Montana 59812, USA.
[8]Department of Physical Geography and Quaternary Geology, Bert Bolin Centre for Climate Research, Stockholm University, SE-106 91, Stockholm, Sweden.
[9]Swedish Nuclear Fuel and Waste Management Co, Box 250, 101 24, Stockholm.
[10]Danish Meteorological Institute, Lyngbyvej 100, DK-2100 Copenhagen Ø Denmark
[11]Department of Geosciences and Natural Resource Management, University of Copenhagen, Øster Voldgade 10, DK-1350 Copenhagen, Denmark.
[12]Alfred-Wegener-Institut Helmholtz-Zentrum für Polar- und Meeresforschung, Am Handelshafen 12, 27570 Bremerhaven Germany
[13]Department of Crystallography, Geoscience Centre, University of Göttingen, Goldschmidtstraße 1, 37077 Göttingen, Germany
[14]Scott Polar Research Institute, University of Cambridge, Lensfield Road, Cambridge, CB2 1ER, UK

*Please address e-mail correspondence to: sdd08@aber.ac.uk

Contents

Introduction
S1. Previous rainfall/melt-induced acceleration events in Greenland
S2. Long-term trends in rainfall seasonality and future predictions

This is the author's post-print. The final version was first published by Nature Geoscience on 13 July 2015, doi: 10.1038/NGEO2482

References
Supplementary figures

Introduction

The supplementary information is structured into two sections. Section S1 identifies and describes three previous rainfall/melt-driven acceleration events on the Greenland ice sheet (GrIS) evident in recent studies. Section S2 investigates long-term trends in rainfall seasonality using the Kangerlussuaq precipitation record and HIRHAM5 regional climate model simulations of the rainfall fraction over the K-transect between 1990 and 2009, before discussing the findings in the wider context provided by recent studies. Supplementary figures follow the reference list, which only includes references that were not cited in the main manuscript. Four supplementary animations are provided as separate files.

8. Previous rainfall/melt-driven acceleration events and their frequency

In this section we describe three pronounced acceleration events evident in previous studies[14,33,34] that can, with hindsight, now be reinterpreted as being driven by cyclonic-induced rainfall and melt. These acceleration events in August 1995, August-September 1997 and August 2006 are indicated on Fig. 5a. It is evident from Fig. 5a that similar events occurred in other years, with the heaviest rainfall events typically occurring in the months of August and September.

8.1. August 1995 event

Asides from the Baffin Bay cyclone responsible for the August-September 2011 event, other synoptic patterns that bring precipitation to widespread areas of south Greenland include the Labrador Sea cyclone and the Southern Tip cyclone[29]. In 1995 a cyclone tracked over the

southern tip of Greenland, advecting warm air, bringing heavy precipitation (Figs. S4 and S10), and driving a widespread acceleration on the Kangerlussuaq sector of the GrIS (see Figure 3 of Ref. 33), which was captured using interferometric synthetic aperture radar (InSAR) on European Remote Sensing (ERS) satellite images[33]. Although Ref. 33 capture and describe the widespread acceleration of up to 360% extending up to 100 km inland they make no mention that it was driven by widespread melt and rainfall under cyclonic weather conditions. Between 3 August and 14 August 1995, 49.8 mm of rain was recorded at DMI station 04231 in Kangerlussuaq, with 10.9 mm on the 11 August[59]. The widespread nature of the precipitation and near surface air temperature anomaly (Fig. S4) suggests the acceleration in ice flow, which was ubiquitous across the Kangerlussuaq sector, occurred over a broad region of the GrIS.

8.2. August/September 1997 event

It is evident from Figure 3 of Ref. 14 that a pronounced, transient uplift and acceleration event occurred at Swiss Camp in late August and early September 1997. Swiss Camp is located 46 km from the terminus of Sermeq Avannarleq in West Greenland (Fig. 1a), ~ 280 km north of Russell Glacier. During this event, surface uplift attained ~ 45 cm above preceding levels and the ensuing acceleration extended enhanced summer velocities into September, a time when in all other years velocities had begun to decline. Further analysis reveals that a Baffin Bay cyclone advected warm air and rainfall over this area of the ice sheet at this time (Figs. S5 and S11). Between 31 August and 6 September, reanalysis data reveal that 20-39 mm of rain occurred over the western margin of the GrIS, with pockets of heavier rain of 40-59 mm over Upernivik and 80-99 mm over southwest Greenland (Fig. S5). Over the same period 10.6 mm of rain was

recorded in Kangerlussuaq[59], and although more rain may have fallen in Swiss Camp it is likely that surface ice melt was the largest contributor to surface runoff during this event. The surface uplift and acceleration event at Swiss Camp in late-August to early-September 1997 occurred during days with a low positive-degree day (PDD) sum (Fig. 3c of Ref. 14) inferring that air temperatures were not particularly high and suggesting that the turbulent heat fluxes and longwave cloud effect were more important for melt production than shortwave solar radiation, as occurred in late August 2011.

8.3. August 2006 event

Another similar rainfall/melt-induced acceleration event on the Kangerlussuaq sector is evident in Figure 3b and c of Ref. 34. As occurred in 2011, the week-long acceleration event in August 2006 resulted in the highest velocities during the whole year at K-transect site SHR (herein named R13; Fig. S7 of the Supplementary Information and Fig. 3b of Ref. 34). The synoptic weather was also comparable to the August-September 2011 event: a Baffin Bay cyclone advected warm, moist air across south Greenland (Figs. S6 and S12). It is pertinent to note that, it was the high melt rate during this event combined with rainfall that drove the acceleration at sites R13 and R38 in August 2006 – and the high melt rate is not portrayed in Figure S7, which shows air temperature, precipitation and velocity. Consistent with reanalysis data (Fig. S6), 10.4 mm of rain fell in Kangerlussuaq between 16 to 22 August 2006, with the heaviest rainfall (7 mm) on 20 August 2006. To our knowledge, melt data are unavailable for this period and simple temperature index models (e.g. Ref. 73), which neglect the turbulent heat fluxes, would not be able to accurately reconstruct the melt rate. We also note that the lack of high velocities during a

second period of rainfall from 22 to 23 August 2006 can be explained by low accompanying melt rates and the presence of efficient subglacial drainage developed during the previous event[12,21].

These three events in 1995, 1997 and 2006 demonstrate that the widespread melt, rainfall and acceleration event resulting from cyclonic weather conditions we observed in late August 2011 was not a one-off. We note that the four acceleration events we have identified are unlikely to be the only events, and that previous heavy rainfall events evident on Fig. 5a are likely to have produced similar widespread accelerations in ice flow on the GrIS.

9. Long-term trends in rainfall seasonality and future predictions

We found an increasing trend in the annual total precipitation, rainfall and snowfall in Kangerlussuaq superimposed on large inter-annual variability (Fig. S8). The linear trend in annual precipitation ($r = 0.27$; $p = 0.10$) and rainfall ($r = 0.29$; $p = 0.08$) are significant at the 90% confidence level. The slight decrease in rainfall from 1990-99 to 2000-09 of 2 mm per year, which is imprinted on a steady linear increase with large inter-annual variability, can be explained by a switch from a positive mean summertime (June-August; JJA) North Atlantic Oscillation (NAO) index between 1990-99 to a negative mean JJA NAO between 2000-09[74]. A negative JJA NAO favours high-pressure and a reduction in the advection of cyclonic weather systems over Greenland, leading to a decrease in overall precipitation during summer. As the majority of rainfall in Greenland occurs during summer this reconciles the seemingly contradictory observations of a reduction in the annual total rainfall from 1990-1999 to 2000-2009 and a contemporaneous increase in the rainfall fraction during summer (Fig. 5c). The rainfall seasonality index shows a decline ($r = -0.21$; $p = 0.21$) from 1.32 in 1980-89 to 1.30 in 1990-99 to 1.22 in 2000-09, indicating that the seasonal distribution of rainfall has become more

dispersed (Fig. S8d). The number of days of rain (> 1 mm) per year also shows an increasing trend ($r = 0.27$, $p = 0.10$) of approximately 3 days per decade (Fig. S8e). The greatest number of rain days occurred in the record warm year of 2012[75] (which exhibited an intensely negative JJA NAO[74]) with 53 days of > 1 mm of rain, which is 2.4 standard deviations above the mean and 0.93 standard deviations above the next highest year (Fig. S8e). Examining the percentile day of year statistics (Fig. 5b) provides insight into the detail of the dispersion: rainfall has become earlier and later in the season between 1980 and 2012, with the IDR increasing by an average of 8 days per decade. The pace of the 10th percentile day of year becoming earlier (3.4 days per decade) was surpassed by the rate of the 90th percentile day of year becoming later (4.9 days per decade) and the dispersion is therefore asymmetric with rain falling disproportionally later in the season. These results are consistent with the HIRHAM5 RCM simulation that indicate an overall increase in the rain fraction across the K-transect from 1990-99 to 2000-09, which is particularly large in August and September (Fig. 5c). These results are further supported by results from a three-model ensemble that predicts the greatest increase in Greenland precipitation during the next century will occur in autumn[4]. The HIRHAM5 RCM results also reveal an increase in the rainfall fraction at high elevations (above 1400 m asl) between these two decades (Fig. 5c) where annually-averaged ice flow increased year-on-year between 2009 and 2012[41]. These findings are further supported by previous climate modelling studies that indicate that the rainfall fraction increased across Greenland between 2000 and 2011[46] and was higher during the anomalously warm year of 2007 (8.5%) compared to the 1990-2008 mean (6.2%)[76]. Under anticipated warmer air temperatures the rainfall fraction is expected to continue to increase over the next century, which would result in a lowering of surface albedo and enhanced surface ice melt[45,46].

This is the author's post-print. The final version was first published by Nature Geoscience on 13 July 2015, doi: 10.1038/NGEO2482

Recent studies suggest that under climate warming, precipitation over Greenland will change in three ways: (i) changes in the frequency of synoptic patterns, (ii) changes in the precipitation that occurs when a certain synoptic pattern occurs, and (iii) changes in the phase of precipitation i.e. the ratio of rainfall to snowfall known as the rainfall fraction. These are expanded below:

i. Ref. 4 found that 83% of the predicted increase in precipitation from 35.8 to 45.0 cm yr^{-1} over Greenland by the end of the 21st century can be attributed to a rise in precipitable water in the atmosphere as a result of higher air and ocean temperatures and reduced sea ice cover. Climate warming is expected to enhance ocean evaporation and the moisture carrying capacity of the air, resulting in an increase in precipitable water and therefore higher precipitation over the ice sheet[44].

ii. The frequency of Baffin Bay cyclones is predicted to increase from 3% of days in 1961-99 to 4% of days in 2081-2100[4]. The frequency of several other cyclonic weather systems over Greenland is also expected to increase with a northward shift in North Atlantic storm tracks[4]. The observed and predicted future increase in cyclonic weather systems over the GrIS, and the Arctic in general, is a theme common to many previous studies[4,5,77-80].

iii. The rainfall fraction is expected to increase under a warmer climate as warmer air temperatures cause more precipitation to fall as rain[45,46,76].

The observed and predicted changes in precipitation are not homogenous across Greenland. Annual snowfall is expected to increase in the interior of the ice sheet, while a substantial proportion of snowfall in south Greenland is expected to turn to heavy rainfall[45,46].

This is the author's post-print. The final version was first published by Nature Geoscience on 13 July 2015, doi: 10.1038/NGEO2482

Supplementary References

73 Hock, R. Temperature index melt modelling in mountain areas. *Journal of Hydrology* **282**, 104-115, doi:10.3189/172756405781812529 (2003).

74 Tedesco, M. *et al.* Evidence and analysis of 2012 Greenland records from spaceborne observations, a regional climate model and reanalysis data. *The Cryosphere* **7**, 615-630, doi:10.5194/tc-7-615-2013 (2013).

75 Nghiem, S. V. *et al.* The extreme melt across the Greenland ice sheet in 2012. *Geophysical Research Letters* **39**, L20502, doi:10.1029/2012gl053611 (2012).

76 Ettema, J. *et al.* Higher surface mass balance of the Greenland ice sheet revealed by high-resolution climate modeling. *Geophysical Research Letters* **36**, doi:10.1029/2009GL038110 (2009).

77 McCabe, G. J., Clark, M. P. & Serreze, M. C. Trends in Northern Hemisphere surface cyclone frequency and intensity. *Journal of Climate* **14**, 2763-2768, doi:10.1175/1520-0442(2001)014<2763:TINHSC>2.0.CO;2 (2001).

78 Schuenemann, K. C. & Cassano, J. J. Changes in synoptic weather patterns and Greenland precipitation in the 20th and 21st centuries: 1. Evaluation of late 20th century simulations from IPCC models. *J Geophys Res-Atmos* **114**, doi:10.1029/2009jd011705 (2009).

79 Sorteberg, A. & Walsh, J. E. Seasonal cyclone variability at 70° N and its impact on moisture transport into the Arctic. *Tellus A* **60**, 570-586, doi:10.1111/j.1600-0870.2008.00314.x (2008).

80 Zhang, X., Walsh, J. E., Zhang, J., Bhatt, U. S. & Ikeda, M. Climatology and interannual variability of Arctic cyclone activity: 1948-2002. *Journal of Climate* **17**, 2300-2317, doi:10.1175/1520-0442(2004)017<2300:CAIVOA>2.0.CO;2 (2004).

This is the author's post-print. The final version was first published by Nature Geoscience on 13 July 2015, doi: 10.1038/NGEO2482

Table S1. Position, elevation, ice thickness and velocity statistics for the GPS sites on Russell Glacier, Isunngata Sermia, Sermeq Avannarleq and Store Glacier. The mean velocity during the event is compared to the mean velocity during the preceding week. Due to the variable timing of the event between glaciers and with distance from the ice margin the event period is defined for each site as the period of enhanced velocities.

	Ice thickness (m)	Mean annual velocity (m yr^{-1})	Preceding velocity (m yr^{-1})	Event velocity (m yr^{-1})	Percentage increase (%)
Russell Glacier GPS sites:					
R2 (383 m asl) N67° 06' W050° 12'	158	100	81	176	117
R13 (732 m asl) N67° 06' W049° 56'	610	113	95	228	140
R38 (1010 m asl) N67° 05' W049° 24'	883	73	68	116	71
R52 (1110 m asl) N67° 00' W049° 09'	923	96	88	144	64
R88 (1520 m asl) N67° 03' W048° 15'	1223	101	83	121	46
Isunngata Sermia GPS sites:					
I14 (635 m asl) N67° 11 W050° 02'	491	130	137	162	18
I27 (894 m asl) N67° 12' W049° 43'	521	100	99	133	34
I46 (1156 m asl) N67° 12' W049° 17'	830	115	99	147	49
Sermeq Avannarleq GPS site:					
A20 (706 m asl) N69° 27' W049° 53'	602	100	73	142	95
Store Glacier GPS site:					

This is the author's post-print. The final version was first published by Nature Geoscience on 13 July 2015, doi: 10.1038/NGEO2482

S11 (468 m asl) N70° 27' W050° 22'	No data	1953	1820	1985	9

This is the author's post-print. The final version was first published by Nature Geoscience on 13 July 2015, doi: 10.1038/NGEO2482

Table S2. Position and elevation of the meteorological stations on Russell Glacier.

Meteorological stations (M) are labelled with the distance from the terminus of Russell Glacier.

Site	Position	Elevation (m asl)
M0	N67° 08' W050° 11'	345
M13/R13	N67° 06' W049° 56'	732
M61	N67° 04' W048° 49'	1280
M140/R140	N67° 00' W047° 01'	1840

This is the author's post-print. The final version was first published by Nature Geoscience on 13 July 2015, doi: 10.1038/NGEO2482

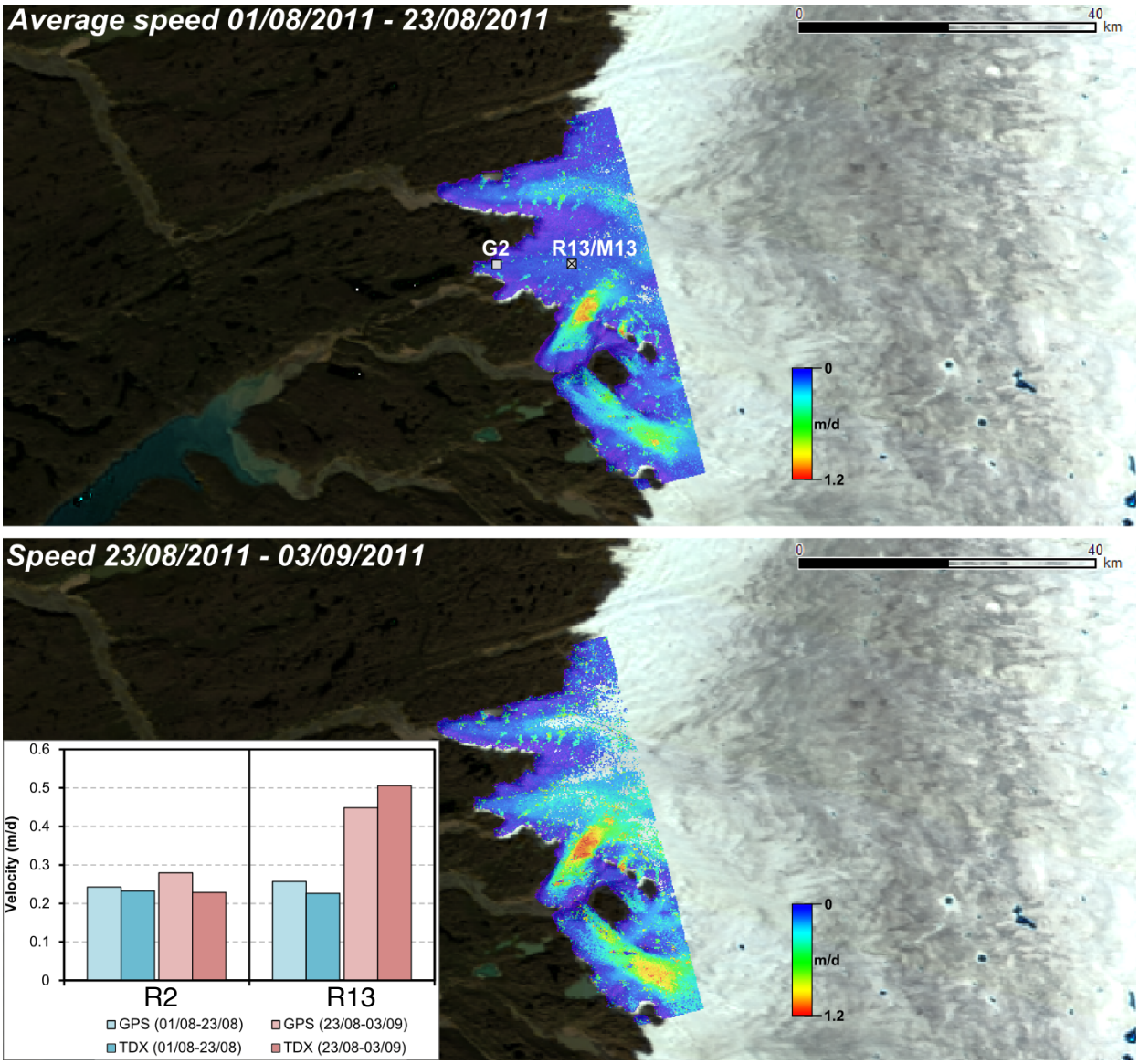

Fig. S1. TanDEM-X velocities during (top) the preceding period (1 to 23 August 2011) and (bottom) the late-August acceleration (23 August to 3 September 2011). The lower-left inset shows the good agreement between TanDEM-X (TDX) and GPS velocities for sites R2 and R13 during both periods.

This is the author's post-print. The final version was first published by Nature Geoscience on 13 July 2015, doi: 10.1038/NGEO2482

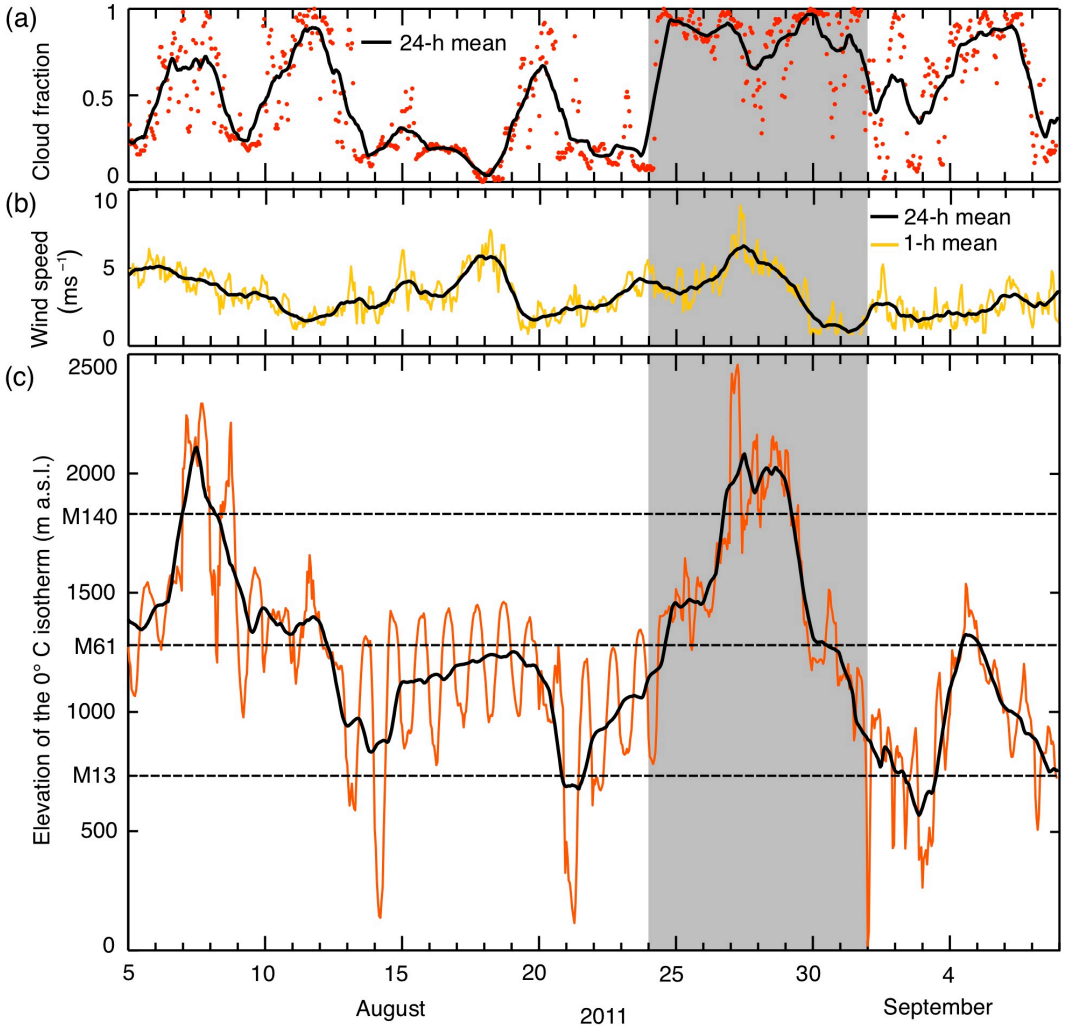

Fig. S2. (a) Hourly estimates of the cloud fraction at M13 (red dots) and the 24-hour running mean cloud fraction, **(b)** 2-m wind speed at M13 with a 1 and 24-hour running mean, **(c)** elevation of the 0° C degree isotherm across Russell Glacier catchment in August and September 2011. Cloud cover was approximated making use of the strong dependence of downwards longwave radiation on atmospheric moisture[58]. The elevations of AWS stations M13, M61 and M140 are plotted on (c) as horizontal dashed lines for reference. The red line is the hourly

freezing level and the black line is the 24-h running mean. The timing of the late-August acceleration is shaded in grey. To allow comparison, the x-axis is the same as that of Figure 3.

This is the author's post-print. The final version was first published by Nature Geoscience on 13 July 2015, doi: 10.1038/NGEO2482

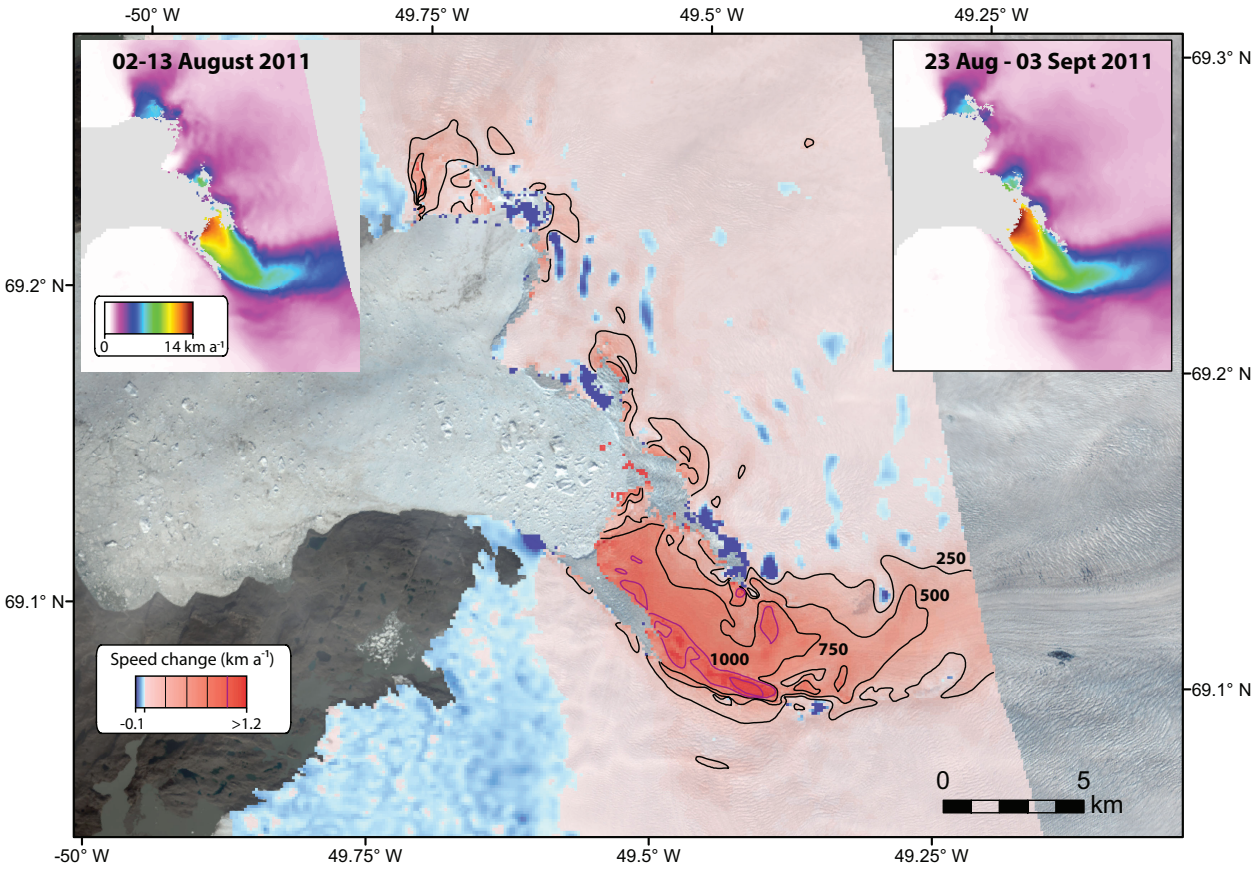

Fig. S3. Velocity difference map for Jakobshavn Isbræ derived from velocity maps created from image pairs acquired on the 2 to 13 August 2011 (inset left) and the 23 August to 3 September 2011 (inset right). The velocity difference is shown by the colour scale and annotated contours; the latter has units of m a^{-1}.

This is the author's post-print. The final version was first published by Nature Geoscience on 13 July 2015, doi: 10.1038/NGEO2482

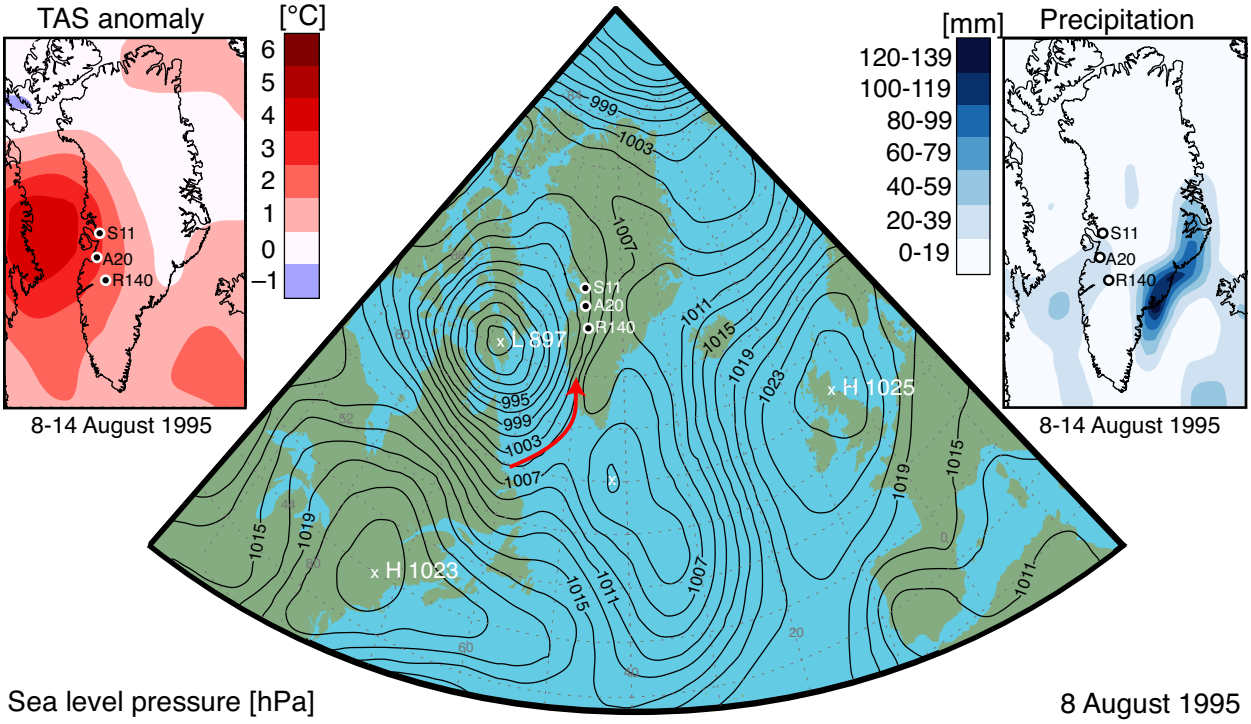

Fig. S4. Reanalysis data[27] for the 1995 event reported in Ref. 33 including sea level pressure for 8 August 1995, the near surface air temperature (TAS) anomaly for the 8-14 August versus the same period in the 1981-2010 baseline, and the total precipitation over the same period. The red arrow shows the direction of warm air advection.

This is the author's post-print. The final version was first published by Nature Geoscience on 13 July 2015, doi: 10.1038/NGEO2482

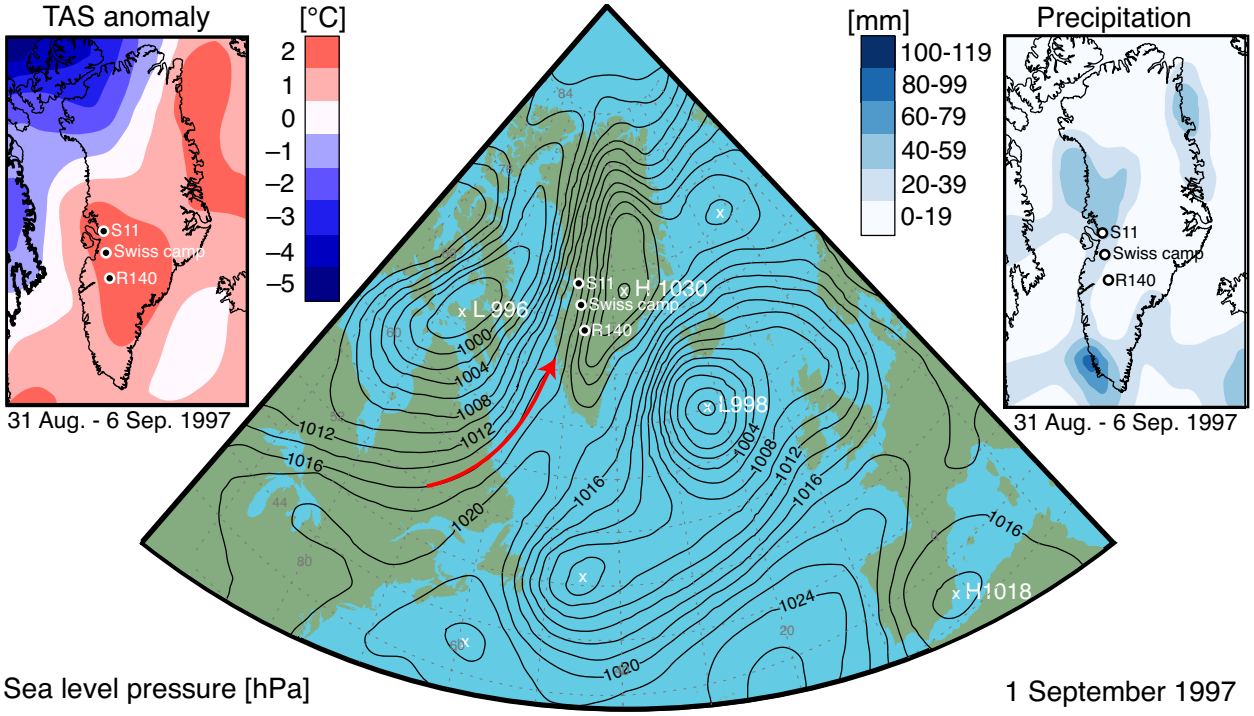

Fig. S5. Reanalysis data[27] for the 1997 event reported in Ref. 14 from Swiss Camp including the sea level pressure for 1 September 1997, the near surface air temperature (TAS) anomaly for the period 31 August to 6 September 1997 versus the same period in the 1981-2010 baseline, and total precipitation over the same period. The red arrow indicates the direction of warm air advection.

This is the author's post-print. The final version was first published by Nature Geoscience on 13 July 2015, doi: 10.1038/NGEO2482

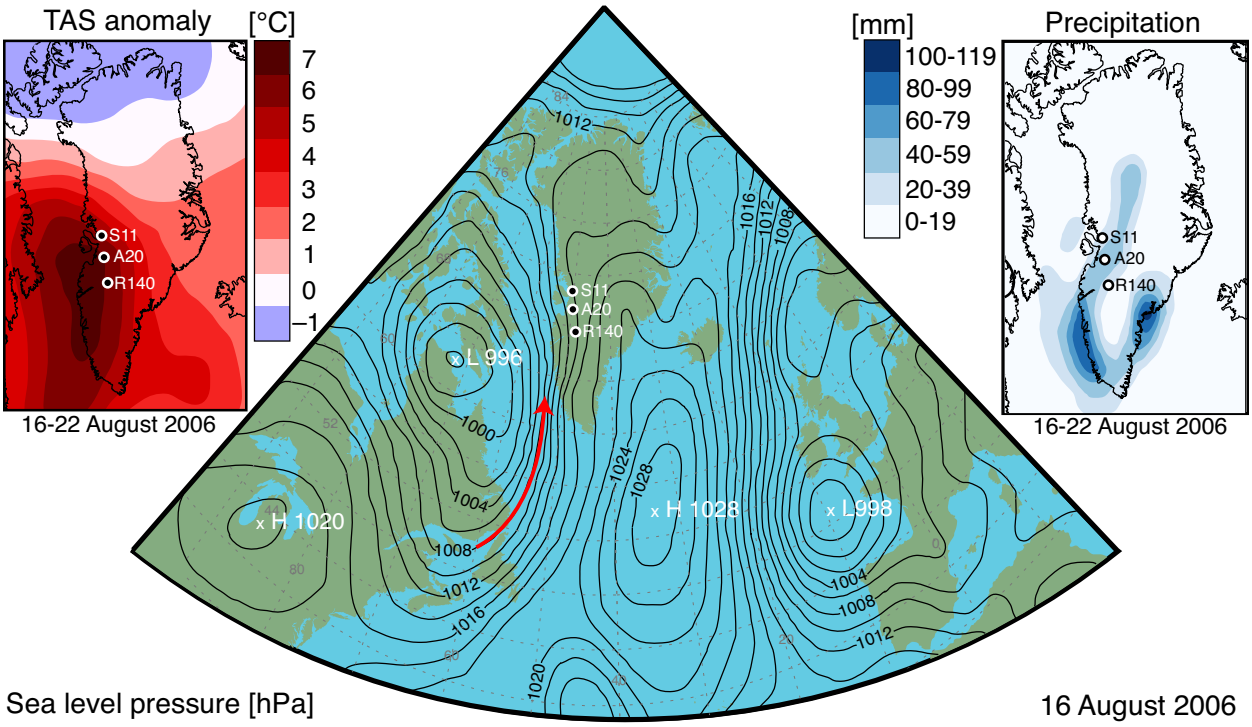

Fig. S6. Reanalysis data[27] for the 2006 event reported in Ref. 34 from the K-transect including the sea level pressure for 16 August 2006, the near surface air temperature (TAS) anomaly for the period 16-22 August versus the same period in the 1981-2010 baseline, and total precipitation over the same period. The red arrow indicates the direction of warm air advection.

This is the author's post-print. The final version was first published by Nature Geoscience on 13 July 2015, doi: 10.1038/NGEO2482

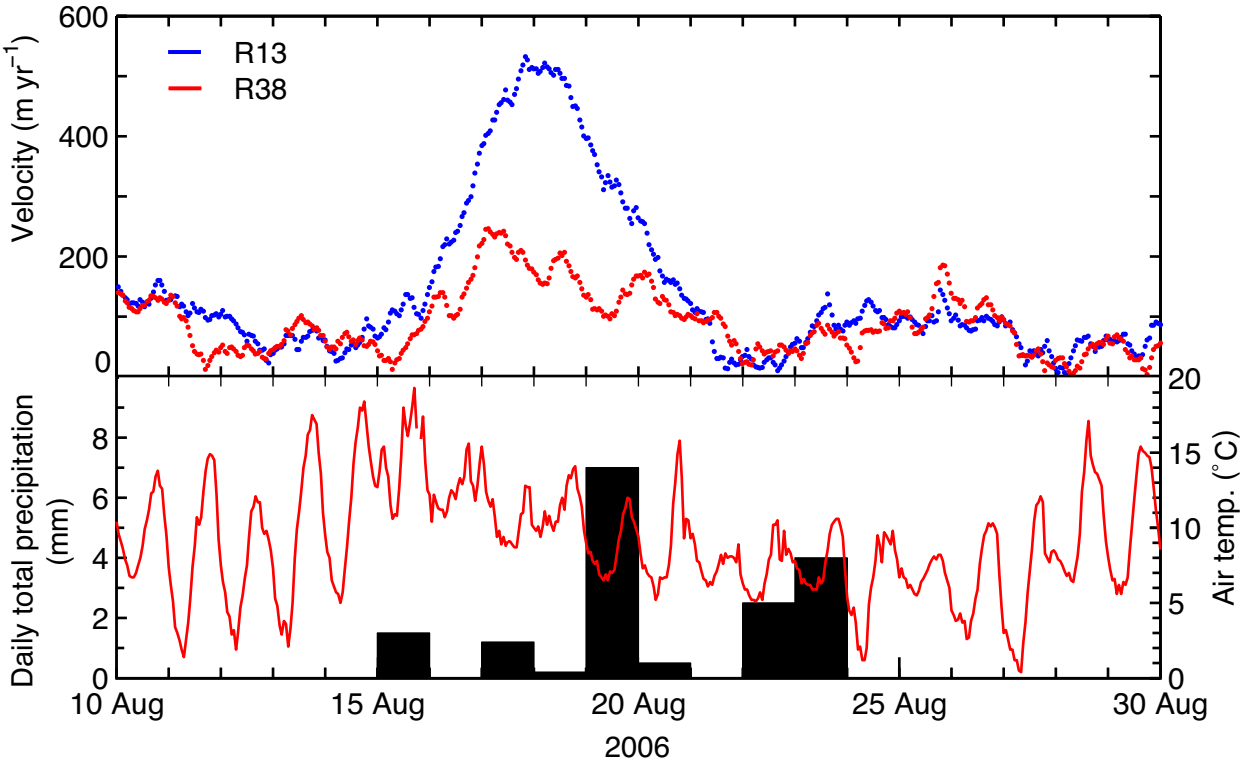

Fig. S7. Precipitation and air temperature in Kangerlussuaq and velocity at GPS sites R13 and R38 during an acceleration event in August 2006. This plot corresponds to Fig. 3d of Ref. 34.

This is the author's post-print. The final version was first published by Nature Geoscience on 13 July 2015, doi: 10.1038/NGEO2482

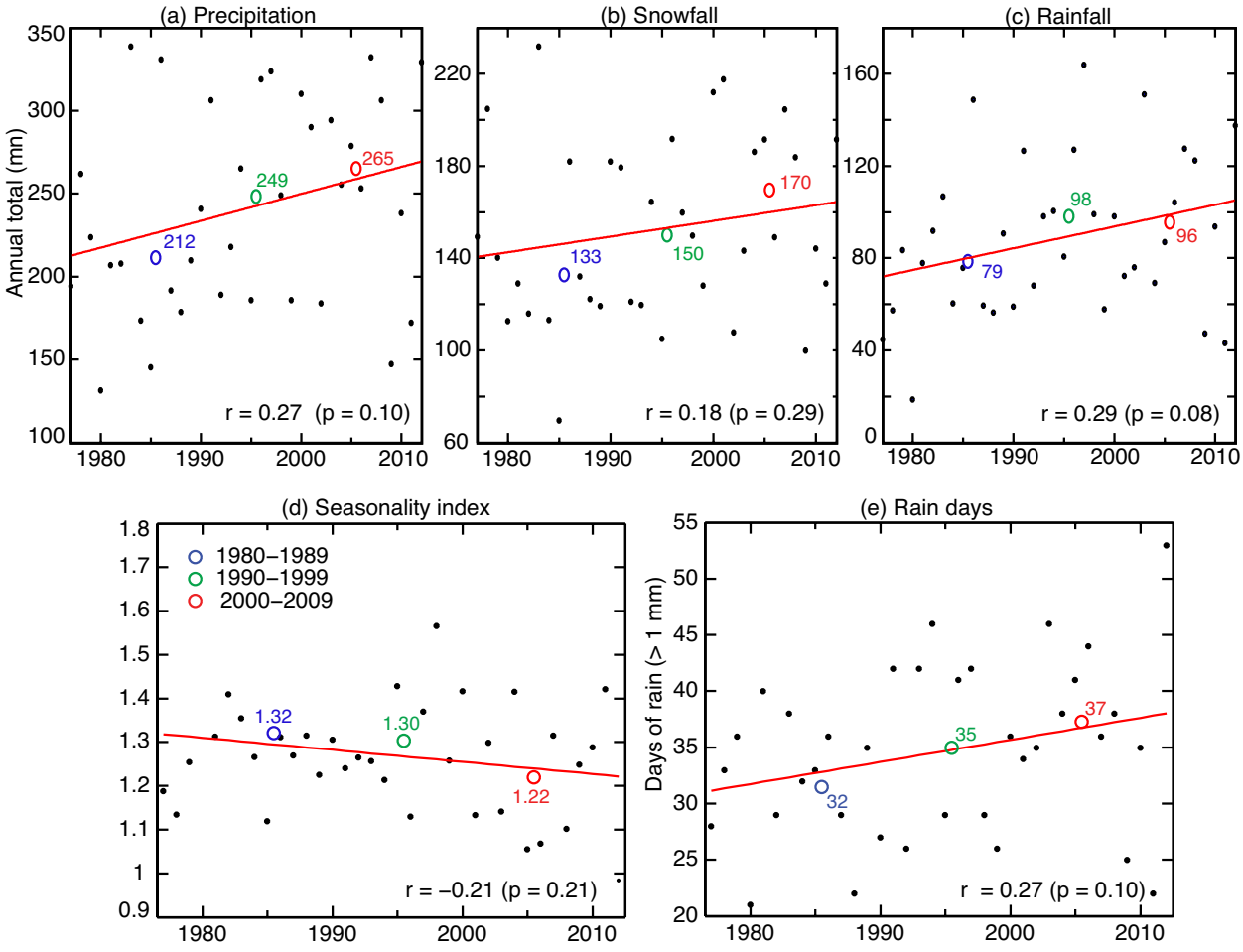

Fig. S8. Trends in the amount, type, seasonal distribution and frequency of precipitation in Kangerlussuaq between 1977 and 2012 including: total annual **(a)** precipitation, **(b)** snowfall and **(c)** rainfall; and **(d)** the rainfall seasonality index, which varies from 0 if all the months have equal rainfall to 1.83 if all the rain falls in one month, and **(e)** the number of days with more than 1 mm of rain per year. Coloured circles show the decadal means and the red line shows the linear trend.